Transports across the 2002 Greenland-Portugal Ovide section and comparison with 1997

P. Lherminier,[1] H. Mercier,[1] C. Gourcuff,[1,2] M. Alvarez,[3,5] S. Bacon,[4] and C. Kermabon[1]

Received 27 June 2006; revised 30 December 2006; accepted 28 February 2007; published 4 July 2007.

[1] The first Ovide cruise occurred in June–July 2002 on R/V Thalassa between Greenland and Portugal. The absolute transports across the Ovide line are estimated using a box inverse model constrained by direct acoustic Doppler current profiler velocity measurements and by an overall mass balance (±3 Sv, where 1 Sv = 10^6 m^3 s^{-1}) across the section. Main currents are studied and compared to the results of the similar Fourex section performed in August 1997 and revisited here. The meridional overturning cell (MOC) is estimated in two different ways, both leading to a significantly lower value in June 2002 than in August 1997, consistent with the relative strength of the main components of the MOC (North Atlantic Current and deep western boundary current). It has been found that the MOC calculated on density levels is more robust and meaningful than when calculated on depth levels, and it is found to be 16.9 ± 1.0 Sv in 2002 versus 19.2 ± 0.9 Sv in 1997. The 2002 heat transport of 0.44 ± 0.04 × 10^{15} W is also significantly different from the 0.66 ± 0.05 × 10^{15} W found in 1997, but it is consistent with the much weaker integrated warm water transport across the section than in 1997.

Citation: Lherminier, P., H. Mercier, C. Gourcuff, M. Alvarez, S. Bacon, and C. Kermabon (2007), Transports across the 2002 Greenland-Portugal Ovide section and comparison with 1997, *J. Geophys. Res.*, *112*, C07003, doi:10.1029/2006JC003716.

1. Introduction

[2] The upper limb of the meridional overturning cell (MOC) in the North Atlantic carries warm, salty water which is progressively cooled and transformed into subpolar mode water and intermediate and deep waters by winter convection in the Labrador, Irminger Sea, and Greenland Sea as well as by transformation on the continental shelves. The lower limb of the MOC carries these cold waters southward. They are modified by entrainment of warmer waters when crossing the bathymetric sills separating the basins. There is also a return surface branch carrying fresh, cold water originating in the Arctic. This MOC is associated with northward heat transport in the North Atlantic, and its variability could be related to European climate change.

[3] The warm, salty water is transported in the North Atlantic Current (NAC) toward the subpolar seas. Its variability has been indirectly studied through observations by *Bryden et al.* [2005], who find in the subtropics a decrease of about 6 Sv (1 Sv = 10^6 m^3 s^{-1}) in the transport of the lower component of the North Atlantic Deep Water since 1957, consistent with the baroclinic deep western boundary current reduction of about 5 Sv seen after about 1990 in the study of *Bacon* [1998a].

[4] In the work of *Bryden et al.* [2005], this long-term variability is compensated by a stronger southward thermocline flow, thus leading to a plausible decrease in the NAC net northward transport. However, these changes are not easily captured with existing observations north of 50°N when one considers the strength of the monthly to interannual variability and the complex relation between the very strong subtropical gyre intensity and the eddy-rich and relatively weak NAC at this latitude. *Curry and McCartney* [2001] find that at higher latitudes, the low-frequency NAC variability is relatively well captured by a transport index based on potential energy anomaly between the Labrador Basin and Bermuda. This index relates to the combined subtropical and subpolar gyre transport variability responding to the North Atlantic Oscillation (NAO) on the decadal timescale and shows a maximum in the early 1990s after a minimum in the 1960s. The authors emphasize the strong nonlinearities that lead to important interannual variability. Following the same general idea, *Häkkinen and Rhines* [2004] compute a subpolar gyre index and exhibit a weakening of the subpolar gyre surface circulation in the late 1990s, found to be the low-frequency response to the NAO and consistent with the study of *Flatau et al.* [2003]. *Hátún et al.* [2005] correlate this circulation weakening to the North Atlantic Current westward shift (also shown by

[1]Laboratoire de Physique des Océans (UMR 6523 Ifremer/CNRS/UBO), Ifremer, Plouzané, France.
[2]CNES, Ifremer, Plouzané, France.
[3]Instituto de Investigaciones Marinas (CSIC), Vigo, Spain.
[4]National Oceanographic Centre (NOC), Southampton, UK.
[5]Now at Institut Mediterrani d'Estudis Avanats (CSIC/UIB), Esporles, Mallorca, Spain.

0148-0227/07/2006JC003716

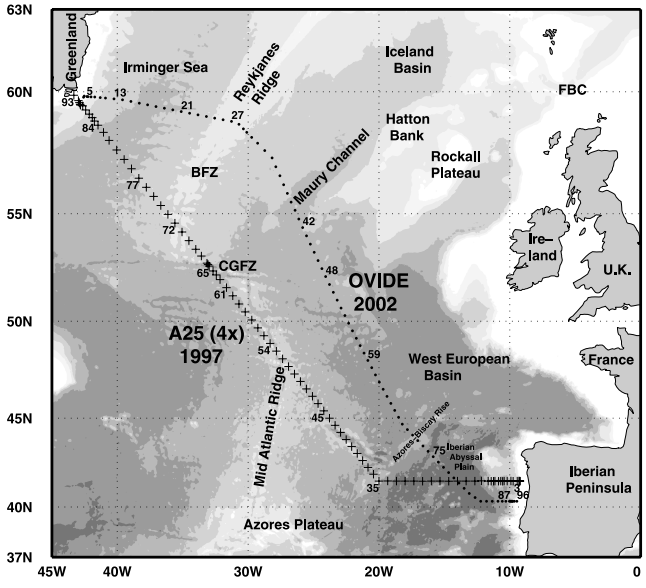

Figure 1. Ovide (squares) and Fourex (crosses) hydrological station locations plotted on bathymetry (500 m intervals). CGFZ: Charlie-Gibbs Fracture Zone; BFZ: Bight Fracture Zone. FBC: Faroe-Bank Channel.

Bersch [2002]) and salinity increase. However, it is not clear that the integrated transport of the NAC shows a correlated variability.

[5] Interannual variability of overflow transport and properties is documented by *Macrander et al.* [2005] in the Denmark Strait and by *Hansen and Østerhus* [2006] in the Faroe Bank Channel. They both show that although the monthly to interannual variability can reach 1 Sv, there is no observable decadal trend. However, hydrological properties of the overflows show an overall freshening that is reported in the paper of *Dickson et al.* [2002] along with all the components of the North Atlantic Deep Water.

[6] The MOC variability is the result of the variability of all the above components. It has been studied mainly in models, where it is generally computed as the maximum of the vertical stream function annual mean. Using hydrographic data, *Koltermann et al.* [1999] and *Bryden et al.* [2005] presented such analyses based on repeat hydrographic sections (at 48° and 25°N, respectively) that intersect the main components of the MOC, and both observed an MOC variability. The Ovide (Observatoire de la Variabilité Interannuelle à Decennale) project aims to repeat a transoceanic hydrographic section from Greenland to Portugal every other year (Figure 1). It is part of the CLIVAR and CARBOOCEAN international programs that are focused on ocean climate variability. The chosen section crosses the main currents implicated in the North Atlantic MOC and is close to the A25 section ("Fourex") of the World Ocean Circulation Experiment performed in 1997. The goal is to contribute to the monitoring of the interannual variability of the water masses as well as the variability of the mass, heat, and tracer transports in the northern North Atlantic Ocean based not only on thermal wind equations and mass balance but also on direct current measurements along the section.

[7] We present an analysis of the Ovide first realization that was carried out in June–July 2002. Results from the 1997 Fourex section discussed in the paper of *Àlvarez et al.* [2004] have been revisited with the same method. Main transports of August 1997 and June–July 2002 could then be consistently compared. A discussion of the estimation and variability of the MOC in these data follows, leading to the calculation of the MOC in potential density coordinates (MOC_σ), which is likely to be the most significant index on such a section for water mass transformation north of the section and for the MOC.

2. Data Set

2.1. CTD Data

[8] The Ovide 2002 cruise was carried out on the French R/V Thalassa. The hydrographic section started on 18 June 2002 off Greenland and ended on 10 July 2002 off Portugal. A total of 104 hydrographic stations were carried out. Only 90 stations (numbers 6 to 96), which form the coast-to-coast section, are used in this work (Figure 1). At the time R/V Thalassa arrived at the tip of Greenland, the shelf was covered with ice, preventing any measurement to be carried out inshore of the 200-m bathymetric contour. The section was interrupted at station 72 for recovering moorings. It was resumed 4 days later at exactly the same location (station 73). Since θ-S properties and currents measured at stations 72 and 73 were acceptably similar, we chose to ignore the latter in our analysis. At the end of the section, measurements were carried out on the Portugal Shelf.

[9] At each station, measurements of temperature, salinity, and dissolved oxygen concentration as a function of pressure were obtained using a Neil Brown Mark III $CTDO_2$ probe. The rosette was equipped with 28 eight-liter bottles. Seawater samples were analyzed on board R/V Thalassa to determine salinity and dissolved oxygen concentration (for $CTDO_2$ calibration purpose), as well as nutrients, CFCs, pH, and alkalinity. The $CTDO_2$ measurement accuracies are thought to be better than 1 db for pressure, 0.002°C for temperature, 0.003 for salinity, and 1 μmol kg^{-1} for dissolved oxygen [*Billant et al.*, 2004]. For further reference, the vertical sections of properties (θ, S, O_2) are shown in Figure 2.

2.2. SADCP Data

[10] Velocity measurements between 32 and 600 m were obtained using R/V Thalassa's RD Instruments 75 kHz Ship Acoustic Doppler Current Profiler, referred to as the SADCP in the following. The four beams of the instrument pinged every 2 or 3 s, and velocity profiles were calculated as ensemble averages of 20 values, after removing the ship velocities. A high level of quality was obtained by using combined navigation data from a differential GPS and two gyrocompasses, and by carefully flagging the data using median filters and tests on the vertical velocity and the velocity error estimate. By comparing currents during the stations and under way, we could crudely verify that the ship velocity was correctly removed. The correlation between the ship velocity and the current component along the trajectory during acceleration phases was then minimized by correcting the ADCP alignment by 0.45°. The correction on measured current velocities is small (less than 0.02 m s^{-1}), but since the ship is always moving in the same direction, the cumulative error without the correction would lead to a

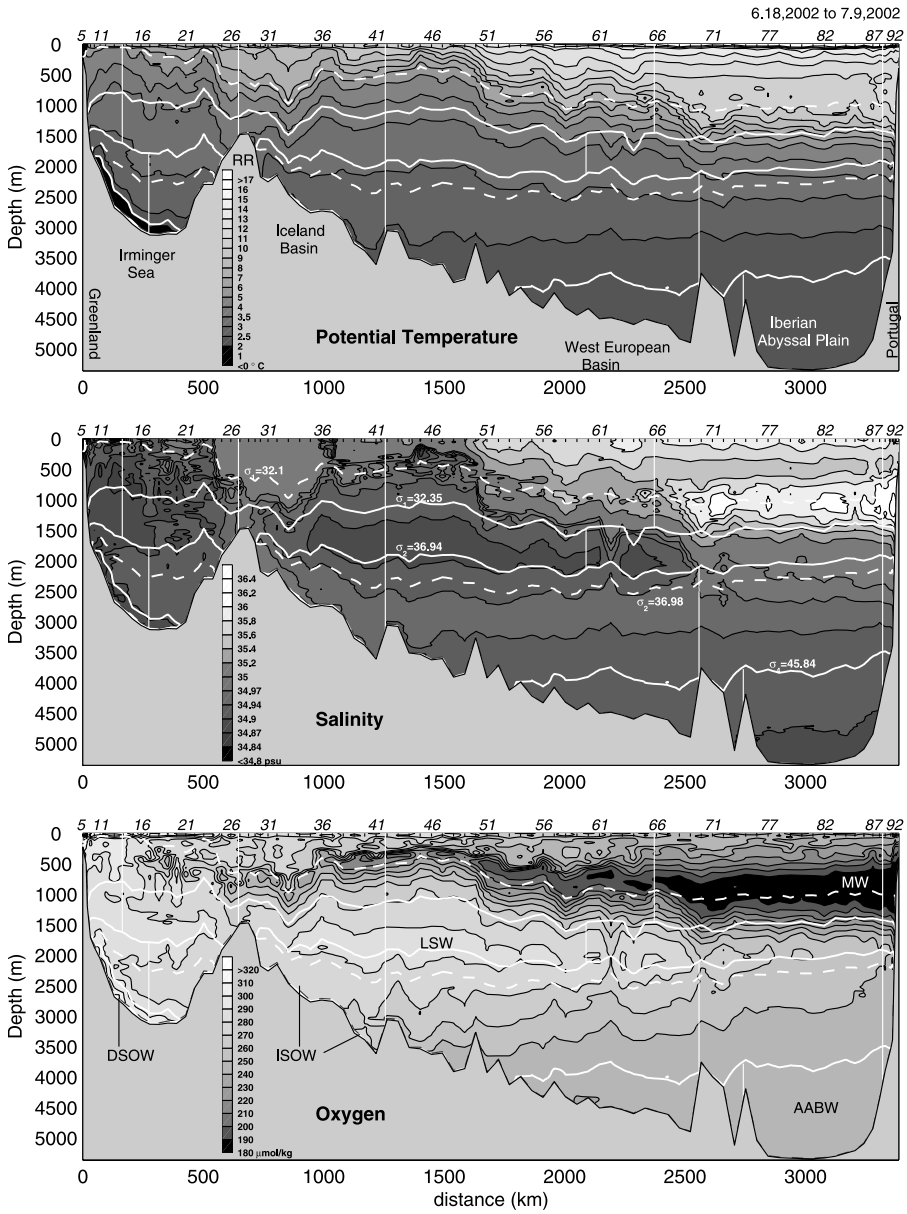

Figure 2. Sections of temperature, salinity, and oxygen along the Ovide line from Greenland (left) to Portugal (right). Isopycnals are drawn in white; continuous lines for σ_1 = 32.35, σ_2 = 36.94, and σ_4 = 45.84 and dashed lines for σ_1 = 32.1 and σ_2 = 36.98. Vertical white lines delimit the main regions of the sections shown in Figure 10. Water masses discussed in the text are shown on the bottom panel: Denmark Strait Overflow Water (DSOW), Iceland-Scotland Overflow Water (ISOW), Labrador Sea Water (LSW), Antarctic Bottom Water (AABW), and Mediterranean Water (MW).

30 Sv transport southeastward. Note however that the data tended to get noisier after station 74, which is most probably a consequence of the oligotrophy of the Iberian Basin water. A section of the East Greenland Current (EGC) is shown in Figure 3. The estimated errors on the 20 ensemble mean velocities are of the order of 0.03 m s^{-1}, showing that the measured vertical velocity is mainly noise.

2.3. LADCP Data

[11] The rosette was equipped with a 150-kHz downward-looking and a 300-kHz upward-looking RD Instruments lowered acoustic Doppler current profiler (LADCP). Both LADCPs returned data at every station. Using the inverse method developed by *Visbeck* [2002], the two data sets were combined to estimate the horizontal velocity profiles at station locations. For 18 stations, data from the 300-kHz upward-looking LADCP were omitted because of their poor quality [*Lherminier et al.*, 2003]. On complex bathymetry features, the influence of the bottom tracking was reduced for 14 stations to the last 50 m instead of 300 m, thus reducing the effect of lateral reflections. Profiles were then studied one by one and compared with the SADCP station-averaged profiles. For 27 stations where comparison was not satisfactory, LADCP profile calculation took into account SADCP data to improve the first 600 m.

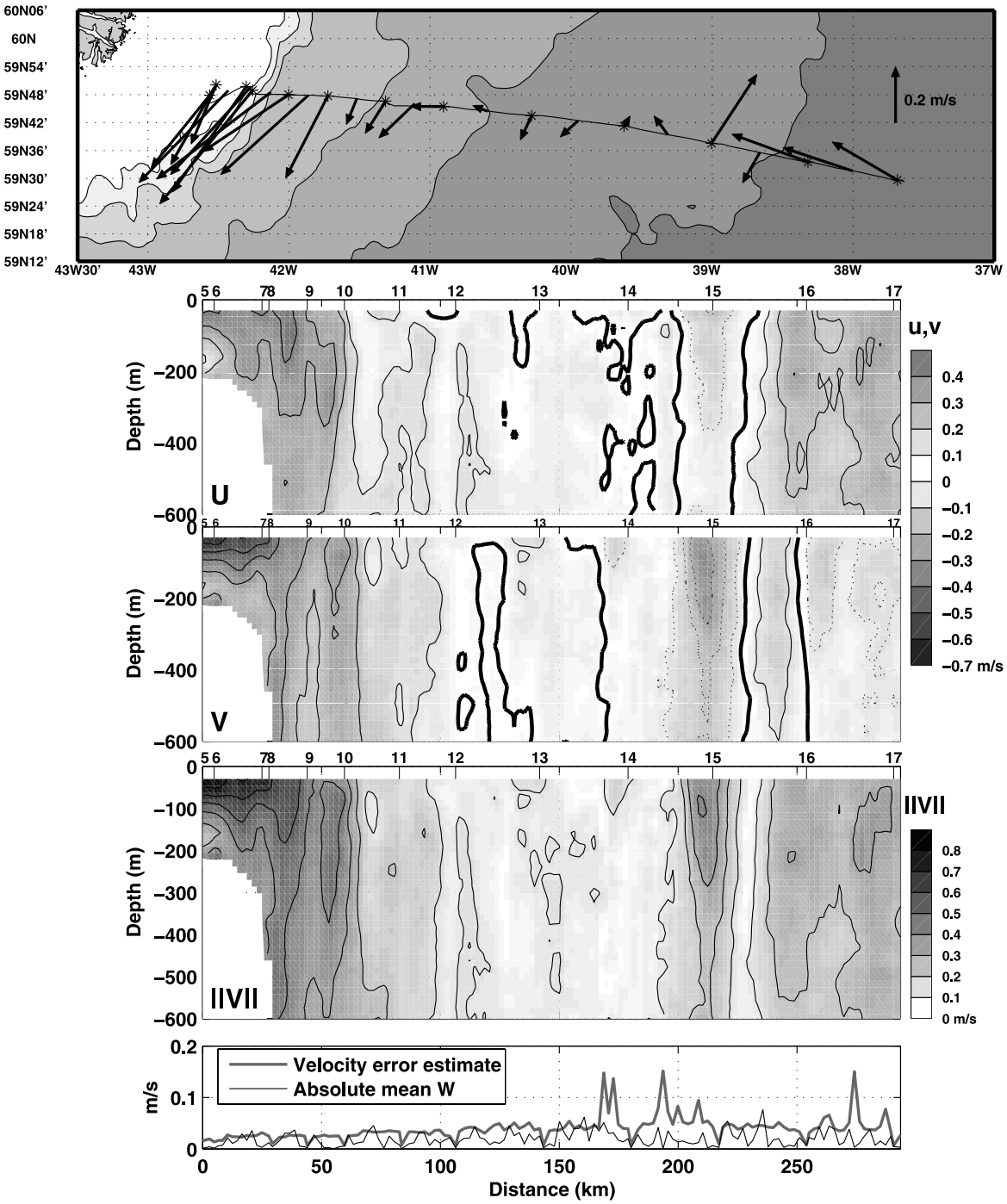

Figure 3. Currents measured by the SADCP. The ship route of the northern part of the section is shown on the first panel on top of bathymetry (500 m intervals). The south tip of Greenland (Cape Farewell) is visible. Stars indicate stations and vectors are local subsurface velocities, averaged between 100 and 200 m and between stations (or for station duration). The three central plots present the zonal (U, positive eastward), meridional (V, positive northward) and absolute ($\|V\|$) velocities as a function of distance (from station 5) and depth. Contours are plotted every 0.1 m s^{-1}; they are dashed for positive values (for U and V only) and bold for the 0 contour. The white patch indicates the seafloor. The bottom plot presents an error estimate on the 20-ensemble mean velocity and an average of the vertical velocity, both between 100 and 400 m.

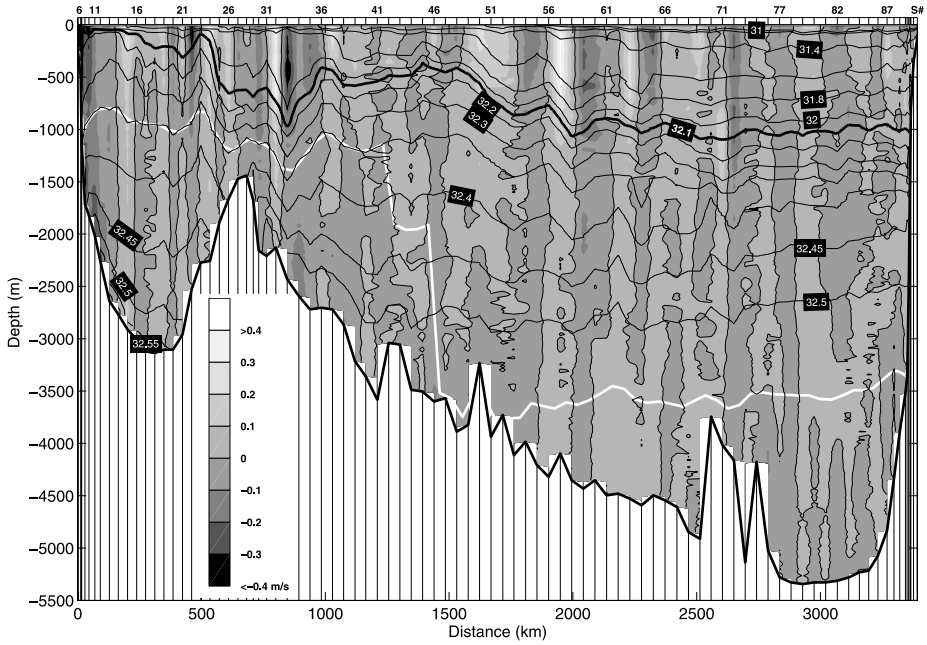

Figure 4. LADCP velocities measured on Ovide 2002 section. Velocities are counted positive northward, and zero contours are underlined. Thin black lines: labeled contours of σ_1 density. Thick white line: reference levels chosen for computing geostrophic velocities.

[12] The section of LADCP currents perpendicular to the Ovide line is plotted in Figure 4. The horizontal gradients of density (see σ_1 isolines in the figure) are consistent with direct measurements of velocities. The subarctic front is noticeable at 1700 km (station 51, 51°N), where the main branch of the North Atlantic Current is measured by the LADCP down to 2500 m depth. The LADCP measurements underline the strongly barotropic character of the currents in the subpolar gyre, contrasting with the more baroclinic structures in the southern part of the section.

[13] For both SADCP and LADCP, the velocity due to the barotropic tide is estimated using the global one-fourth-degree tide model of *Egbert et al.* [1994]. Although the resolution is not suitable on the shelves, we observe that tide currents explain most of the bottom currents on the Iberian shelf as expected. This is not so clear on the Greenland shelf, as it will be discussed in subsection 4.2, but we prefer to simply keep the correction as is. All the discussions below use detided current data, explicitly noted otherwise.

2.4. ADCP Velocity Profiles

[14] Comparison of on-station SADCP and LADCP velocity profiles is useful to check the quality of the data. Then the averaged profiles between stations are compared to geostrophy, and differences are interpreted, as explained hereafter on three examples. Note that for a pair of stations, the SADCP mean profile can be either (a) the average of on-station data, which is then directly comparable to the LADCP mean profile, or (b) the average of the between-station data. We will show that the latter method is naturally more comparable to geostrophy.

[15] When the circulation is barotropic, the direct velocity measurements differ significantly from the geostrophic profiles computed assuming a level of no motion. This statement is illustrated by pair 6 (Figure 5) in the East Greenland Current, where all ADCP average profiles show a good agreement but are shifted from the geostrophic profile although the shear is similar between 100 and 1000 m.

[16] Profiles averaged along the route (dashed in Figure 5) can be very different from those averaged on the stations. This is mainly explained by the station spacing of 47 km (reduced to 23 km on steep topography features, and 37 km in the Irminger Sea): Any mesoscale feature less than 100 km wide can be missampled. It can be seen on the eastern side of the Reykjanes Ridge (RR) with the LADCP profiles of stations 32 and 33 (pair 29 in Figure 5): The ship crosses a 1000-m-deep eddy that has a diameter of 100 km and velocities of about 0.4 m s^{-1}, but the structure is not symmetrically sampled, so the SADCP average along the route differs by 0.2 m s^{-1} from the station averages (from SADCP and LADCP). In this situation, the average along the route is more consistent with the shear of the geostrophic profile. Note that for this pair, SADCP data were not used to improve LADCP profiles in the surface layer, and the agreement is nevertheless very good.

[17] In the Iberian Abyssal Plain, LADCP velocity profiles were used to confirm the chosen reference level for the geostrophic calculation, as illustrated by the crosses on pair 78 of Figure 5.

3. Estimating the Absolute Velocities With the Inverse Model

3.1. Ekman Transports

[18] The Ekman transports across the Ovide line are calculated from the wind stress of the European Centre Medium-Range Weather Forecast reanalysis ERA40 [*Uppala et al.*, 2005]. The value of -0.95 ± 0.51 Sv was obtained by averaging June and July 2002.

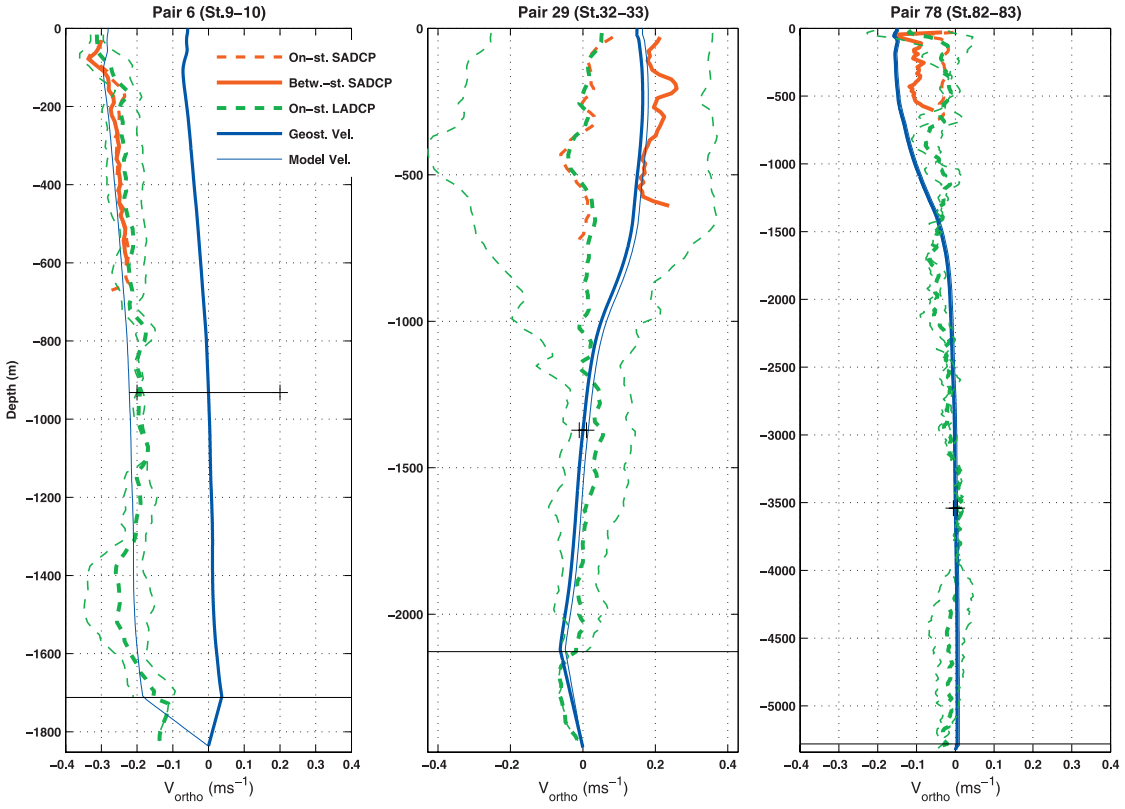

Figure 5. Profiles of the velocity perpendicular to the section at three pairs of stations. The red lines are the velocities measured by the SADCP: the average along the route between the stations is the thick line, and the average of the velocities at both stations is the dashed line. In green dashed lines are the velocities measured by the LADCP on the rosette: Both stations are represented by the thin lines, and the average is depicted by the thick line. The blue lines are the geostrophic profiles: a priori (thick) and after inversion (*S*-sadcp, thin). The horizontal thin line delimited by two crosses shows the $0 \pm \sigma^i$ range at the reference level for geostrophy. The other horizontal black line indicates the deeper common depth of the pair of stations.

3.2. The Box Inverse Model

[19] The absolute geostrophic velocity field perpendicular to the Ovide section was estimated using the following steps. First, geostrophic velocities referenced to selected levels were computed for each station pair. Then, the unknown velocities at the reference levels were estimated by minimizing the weighted sum of the following:

[20] 1. The squared reference level velocities,

[21] 2. The squared residuals of transport constraints derived from the SADCP and LADCP measurements, and

[22] 3. The squared residual of an overall mass conservation constraint.

[23] Noting u_r^i as the unknown reference level velocity at station pair i, $T_{adcp}^{i,k}$ as the SADCP- or LADCP-derived transports at station pair i for a depth interval denoted as k, $T^{i,k}$ as the corresponding model transports, and R as the residual of the mass constraint, then the u_r^i minimize:

$$\sum_{i=1}^{n\,\mathrm{pair}} \left(\frac{u_r^i}{\sigma^i}\right)^2 + \sum_{i=1}^{n\,\mathrm{pair}} \left(\frac{T^{i,k}(u_r) - T_{adcp}^{i,k}}{\sigma_{adcp}^{i,k}}\right)^2 + \left(\frac{R(u_r)}{\sigma_R}\right)^2$$

where σ^i is the expected amplitude of the velocity at the reference level at station pair i, $\sigma_{adcp}^{i,k}$ is the uncertainty on the estimate of the ADCP-derived transport at station pair i for the depth interval k, and σ_R is the error on the mass conservation constraint. "n pair" is the number of station pairs along the Ovide line.

[24] This method is often referred to as the "generalized least square inverse." It allows the computation of errors on reference level velocities [*Mercier*, 1986] and transports [*Lux et al.*, 2000]. Errors on mass and heat transports only include final uncertainties on the reference level velocities. The uncertainties (σ) implemented in the model are discussed hereafter. Transports crossing the section northeastward are counted positive.

3.3. Reference Levels

[25] The reference levels (Figure 4) were first chosen to produce reasonable deep circulation schemes before inversion. In the Irminger Sea and over the eastern flank of the Reykjanes Ridge, the reference levels were set at $\sigma_1 = 32.35$ or at the bottom if shallower. Such a reference level, close to 1000 m, produces a deep cyclonic circulation in the Irminger Sea, in agreement with the study of *Bacon* [1998a]. This choice is close to the minimum current intensity observed in the LADCP data between the East Greenland Current above and the deep western boundary

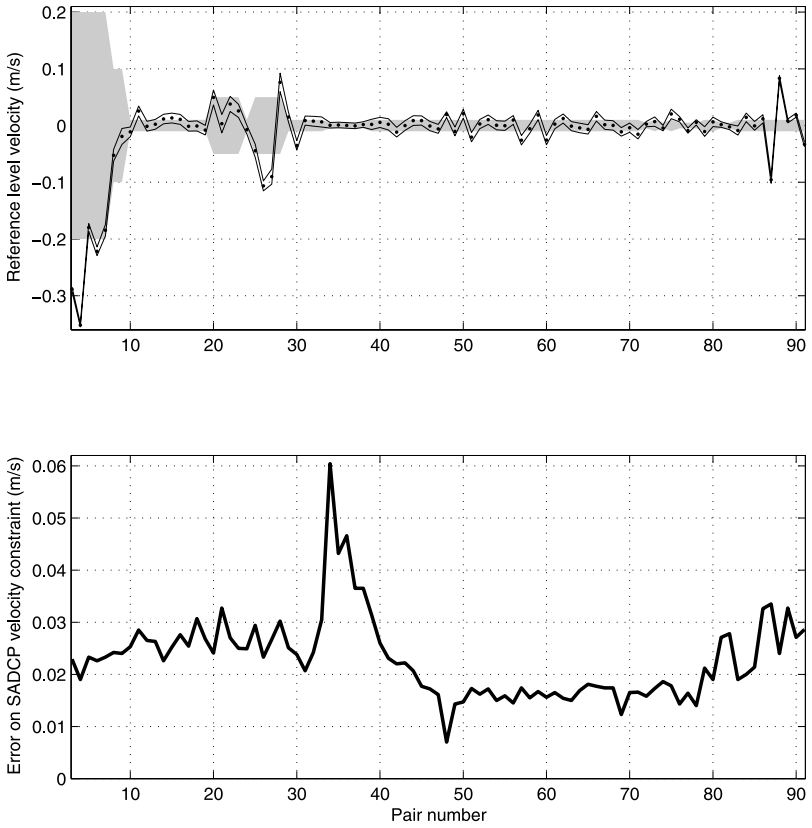

Figure 6. Top: for each pair of station numbered from 3 to 91, velocities at the reference level with errors from the inverse model solution *S*-sadcp, on top of σ^i, the expected amplitude as set in the model (grey area). Bottom: calculated errors on SADCP mean velocity between 86 and 310 m (or bottom). These values are transformed into transport errors $\sigma^{i,k}_{\text{adcp}}$ and implemented directly into the inverse model.

current (DWBC) below. In the West European Basin and the Iberian Abyssal Plain, the reference level was chosen at σ_4 = 45.84 or at the bottom if shallower following the work of *McCartney* [1992]. It gives a net northward geostrophic flow of Antarctic Bottom Water (AABW) of 1.3 Sv, which is a typical value for this water mass transport [*McCartney*, 1992; *Saunders*, 1987]. From stations 42 to 46, the reference levels were chosen at σ_2 = 36.94, consistent with LADCP measurements.

[26] As explained above, the assumption of no motion at the reference level is weighted by the standard deviation σ^i which takes into account the direct current observations. It is chosen wider on the western boundary and around Reykjanes Ridge, where currents are more barotropic (Figure 6).

3.4. Overall Mass Constraint

[27] The mass constraint requires that the sum of the geostrophic and Ekman transports perpendicular to the Ovide line be equal to 1 Sv northward. This value is consistent with the algebraic sum from the 0.8 ± 0.1 Sv inflow through Bering Strait [*Woodgate and Aagaard*, 2005], the 2.6 ± 1 Sv export through Davis Strait [*Cuny et al.*, 2005], and the 0.2 Sv estimate for $P - E + R$ in the Arctic [*Serreze et al.*, 2006]. This constraint is also supported by model estimates of the transport from the subpolar seas into the Arctic Ocean [*Maslowski et al.*, 2004].

[28] A net error of σ_R = 3 Sv is applied to the mass balance, following the analysis of *Ganachaud* [2003], where it is shown that the ageostrophic variability of the ocean is predominant over the nonsynopticity of the measurements in this error estimate.

[29] As a matter of fact, imposing 0, 1 or 1.5 Sv northward for the overall mass balance has no significant impact on the result, as expected from the associated 3 Sv error.

3.5. SADCP Constraints

[30] Considering the sampling issues raised in subsection 2.4, it has been decided to mainly use the SADCP averaged along the ship route to constrain the model. Mass transports can be calculated between 86 and 310 m (or bottom) depths for the 89 pairs of stations by multiplying the measured mean velocity by the distance between stations times the layer thickness. This layer was chosen far enough from the surface to neglect the Ekman contribution and above the depth where the signal-to-noise ratio weakens.

[31] Estimating the transport estimate uncertainties $\sigma^{i,k}_{\text{adcp}}$ is important for the following study since it conditions the influence of the SADCP data on the final results. The uncertainties has two sources: One is due to the instrumental error, and the other is due to the physical environment, i.e., ageostrophic (mainly inertial-gravity waves) and fine-scale currents, which scaling is assumed to be smaller than a

few kilometers. For each pair of stations, the between-station route is divided into N independent 5-kilometer segments. The velocity standard deviations (std) are calculated between 86 and 310 m depths for all the segments, representing the contributions of the two uncertainty sources. The velocity uncertainty is then deduced from the vertical and horizontal averages of the std values divided by $\sqrt{N}$. Uncertainties are found between 0.01 and 0.06 m s^{-1} for the whole section (Figure 6). They are quite representative of meteorological conditions, with rough seas associated with larger error for pairs 34 to 39, and of the decreasing backscatter in the southern part of the section.

[32] For seven pairs of stations in the Iberian Abyssal Plain, SADCP data were unreliable because scattered occasional gaps led to an inappropriate sampling of the velocities along the route. In these cases, we chose to reduce the tolerance on the velocity at the reference level, thus reinforcing the hypothesis of no motion at this level. The pair 78 on Figure 5 is one of these pairs. For all of them, we could verify that LADCP-measured velocities are close to zero at the reference level, as shown by the crosses on the figure.

[33] The inversion, referred to as *S*-sadcp in the following text, uses the SADCP transports between 86 and 310 m depths and the mass conservation to constrain the model at all station pairs.

3.6. LADCP Constraints

[34] Using LADCP velocity profiles to add information to the model is not straightforward when one considers the sampling issue explained in subsection 2.4. There are also other sources of local noise due to a lack of scatterers in the water and to the influence of ageostrophic currents. While weak backscattering levels are more noticeable at depths below 2000 m, the first 1000 m is affected by small-scale baroclinic currents as could be observed by comparing geostrophic vertical shear with LADCP measurements. For instance, internal tides can be seen on steep topographic features. Thus constraining the model with individual profiles introduces inconsistencies with the geostrophic transport estimates.

[35] Instead of constraining the model by individual station pair data, a more satisfying solution is found by calculating LADCP integral transports for seven regions and two layers (separated by $\sigma_2 = 36.95$). Table 1 gives the corresponding transport values used in the inverse model. The regions have been carefully chosen to describe the main current systems and, therefore, to add useful information to the geostrophic estimates. The transport errors $\sigma^{i,k}_{\mathrm{adcp}}$ are estimated by incorporating a sampling error calculated as the RMS of the transport differences between the two stations of the pairs. On the basis of the overall mass balance of the LADCP section, a 0.001 m s^{-1} bias error is included in the error estimates listed in Table 1.

[36] The inversion referred to as *S*-ladcp hereafter uses the LADCP transports of Table 1.

3.7. Summary of Model Setup

[37] The solution of the model that only takes into account the overall mass constraint of 1 ± 3 Sv is referred to as *S*-geost. In the solutions *S*-sadcp and *S*-ladcp, the current measurements were added as constraints for each pair of stations in *S*-sadcp or for seven regions and two layers in *S*-ladcp. In all the following discussion on transports, the *S*-sadcp solution is used, explicitly stated otherwise.

Table 1. LADCP Transports and Errors by Region in Sv[a]

Region	Layer	Stations	Transport
East Greenland C.	Layer 1	5–14	−28 ± 4
Deep Western B. C.	Layer 2	5–17	−9 ± 3
Irminger Sea	Layer 1	14–27	+19 ± 11
Irminger Sea	Layer 2	17–27	+4 ± 4
East Reykjanes	Layer 1	27–42	−18 ± 14
Iceland Scotland O. W.	Layer 2	27–42	−13 ± 3
North Atlantic C.	Layer 1	42–62	+19 ± 11
North Atlantic C.	Layer 2	42–62	−10 ± 6
North Atlantic C. 2	Layer 1	62–75	+8 ± 15
North Atlantic C. 2	Layer 2	62–75	+8 ± 8
Iberian Basin	Layer 1	75–87	−8 ± 8
Antarctic Bottom W.	Layer 2	75–87	−3 ± 10
Eastern B. C.	Layer 1	87–96	+5 ± 2
Eastern B. C.	Layer 2	87–96	−1 ± 3

[a]Layer 1 is defined from the surface to $\sigma_2 = 36.95$, while layer 2 is determined from $\sigma_2 = 36.95$ to the bottom. Regions are plotted in Figure 2. "B." states for Boundary, "C." for Current, "O." for Overflow, and "W." for Water.

4. Transports

4.1. The Vertically Cumulative Transport

[38] The vertically cumulative transports of *S*-sadcp are discussed hereafter (Figure 7). The salinity allows us to identify the water masses that dominate in the water column.

[39] In June 2002, the East Greenland Coastal Current (EGCC), flowing southward, carried ice that prevented any measurement over the shelf but highlighted the role of this current for the freshwater balance of the Arctic [*Bacon et al.*, 2002]. At the northern tip of the section, the low salinity indicates the influence of the EGCC. Between stations 7 and 6, the surface salinity decreases from 33.35 to 32.35, which corresponds to the salinity at the eastern edge of the EGCC in 1997 [*Bacon et al.*, 2002]. Since the 215-m-deep western station (6) is just inshore of the shelf break, we suppose that the EGCC was not fully sampled in 2002 due to the ice cover, and according to *Wilkinson and Bacon* [2005], we expect to miss at most 0.7 Sv flowing southward. This 0.7 Sv is therefore added to the final transport uncertainties in the model solutions.

[40] Away from the shelf, the whole current system in the Irminger Sea is characterized by a mean salinity between 34.88 and 34.92 with a marked cyclonic circulation. On its southeast edge, the aforementioned anticyclonic circulation around the Reykjanes Ridge (RR) between stations 25 and 31 is in the immediate vicinity of a strong anticyclonic mesoscale feature between stations 31 and 34 (see also Figure 2). Traveling toward the southeast, the next noticeable feature is the already mentioned North Atlantic Current beginning at station 48, and followed by three mesoscale patterns centered on stations 53, 58 and 64, whose transports are more easily quantified in Figure 8. The positive salinity anomaly at station 72 centered around 1000 m depth (Figure 2) is wrapped by a strong anticyclonic circulation of 8 ± 4 Sv, which is consistent with the description of a 100-km-wide meddy, and marks the northern limits of the

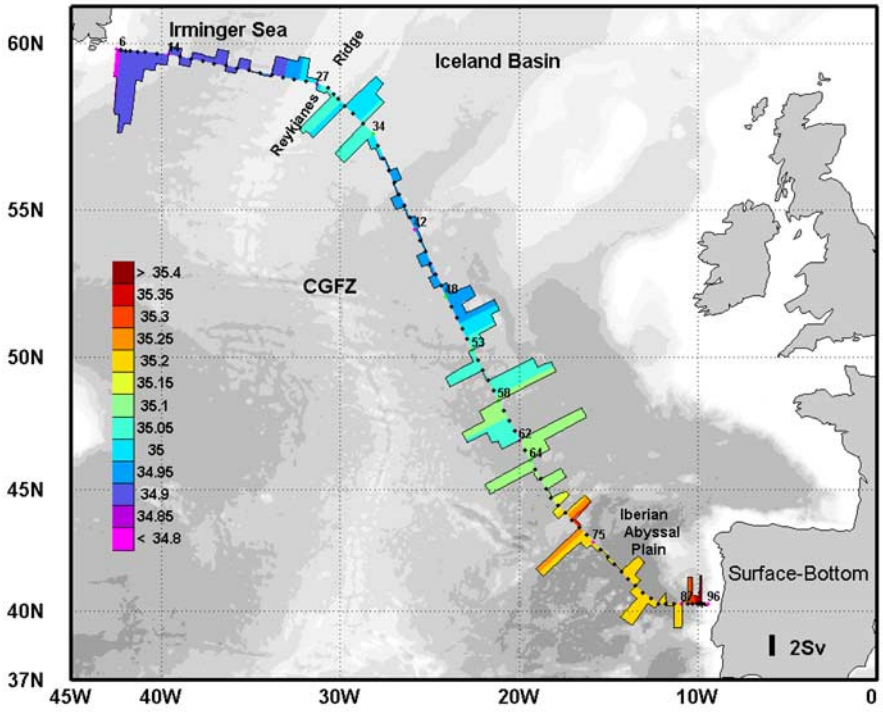

Figure 7. Vertically cumulative transports calculated from the *S*-sadcp run and plotted on the North Atlantic bathymetry, overlaid with the mean salinity of the water column at the corresponding location (in color). The dots are the stations.

Iberian Abyssal Plain and of the Mediterranean Water spreading across the Ovide section. The other salinity anomalies are not easily associated with any particular circulation patterns that could lead us to identify them as isolated structures. The last noticeable feature is the 2.1 ± 0.4 Sv eastern boundary current on the Iberian slope and shelf between stations 89 and 96.

[41] The same circulation patterns can be observed in Figure 8, where transports have been accumulated from Greenland to Portugal. From this figure, we observe a residue of +12 Sv in the geostrophic measurements and −25 Sv in the LADCP cumulative transports. The most significant bias of the latter is caused by stations 32–33 discussed with Figure 5. However, another similar sampling error occurs in an eddy of the DWBC (stations 15–16) and affects the western current system in the Irminger Sea; this quite barotropic eddy can actually be seen in Figure 3. Note that despite these issues, integrating directly measured current data by region allows us to obtain two similar results for *S*-sadcp and *S*-ladcp. By incorporating the current data, we get a more barotropic Irminger Gyre, the magnitude of which is increased from 8 to 20 ± 4 Sv. The circulation around the RR found in most models [*Treguier et al.*, 2005] and in float data [*Lavender et al.*, 2000] is also greatly enhanced, leading to a total transport of 7–13 Sv centered on station 27 (the top of the ridge). Next to it, the anticyclonic circulation magnitude reaches 10 ± 5 Sv. Southeast of RR, the influence of the ADCP data decreases, as would be consistent with a more baroclinic circulation.

[42] The transports for the upper and lower layers are presented in Figure 9. The limit between the layers was fixed at σ_2 = 36.94; this isopycnal is very similar to the usual σ_0 = 27.8 limit in the northern half of the section, and it has the advantage of not varying rapidly along track in the southern half, where it lies around 2000 m depth. Note that it is also located in the core of the Labrador Sea Water, as indicated by the relative minimum of salinity and maximum of oxygen in Figure 2c. To better localize large-scale features in Figure 9, the transports were filtered with a 200-km low-pass filter along the section. In order to analyze the transports by region, the upper and lower layers are subdivided in two layers in Figure 10. The four resulting layers are delimited by σ_1 = 32.35 (above the LSW and similar to σ_2 = 36.874 of the work of *Bacon* [1997]), σ_2 = 36.94, and σ_4 = 45.95 (above the Antarctic Bottom Water). All these figures will be used to describe the main circulation patterns in June 2002.

4.2. Upper Layer Circulation (σ_2 < 36.94)

[43] It is believed that barely 2 Sv of the East Greenland Current (EGC) comes from the Nordic seas fresh boundary current, and a major part of this current at 60°N derives from the Irminger Current circulating from the RR and entraining Irminger Sea Water on its way [*Pickart et al.*, 2005]. That is why, at this latitude, the EGC is also called the East Greenland/Irminger Current (we will keep EGC for simplicity in the following). Property sections definitely show strong salinity gradients within the current that both drive the geostrophic flux and testify to the dual origin of the EGC. This strong current is relatively narrow (165 km width, between stations 6 and 14) and extends from the shelf break and the 2800-m isobath. When calculated above the σ_2 = 36.94 isopycnal, its transport is estimated at 22 Sv southward (Table 3). *Bacon* [1997] estimated 21 Sv for the

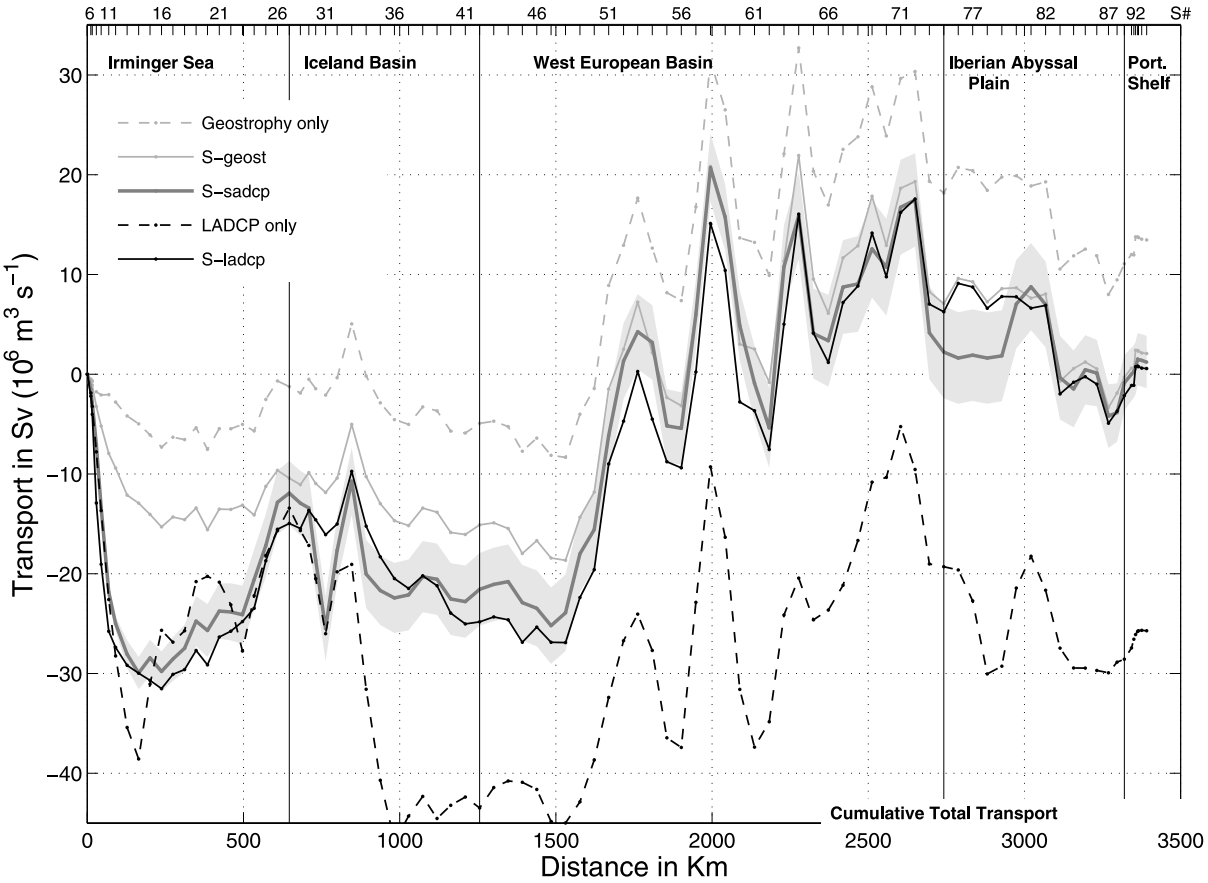

Figure 8. Vertically integrated cumulative transport from Greenland (left) to Portugal (right), plotted against distance along the Ovide section, with station numbers labeled at the top of the plot. Positive values indicate northward transport. The geostrophic (dashed grey) and LADCP (dashed black) transports are from data only. The three other lines are from model inversions: light grey with mass conservation as the only constraint (*S*-geost), thick dark grey with mass conservation and SADCP constraints on each pair (*S*-sadcp), and black with mass conservation and LADCP constraints by region (*S*-ladcp). The shaded region indicates the uncertainty in the *S*-sadcp solution.

EGC transport at 60°N (from the surface down to σ_2 = 36.944). This value is surprisingly similar considering the known variability of the East Greenland Current at short timescale, but models also show that this variability is minimum in summer, consistent with a weaker wind forcing [*Treguier et al.*, 2006]. Furthermore, *Bacon* [1997] also uses ADCP data and an inverse model to obtain this value, and the overall mass transport constraint used in both models tends to damp the variability at very short timescale (a few days).

[44] The cyclonic Irminger gyre is well defined in the circulation schemes derived from surface drifters [*Fratantoni*, 2001; *Reverdin et al.*, 2003; *Flatau et al.*, 2003]. During Ovide, the signature of this cyclonic circulation was a doming of the isotherms and isopycnals between stations 5 and 26 (Figure 2a), a feature that might favor local convection during severe winters [*Bacon et al.*, 2003; *Pickart et al.*, 2003]. In the same figure, the oxygen section shows a relative maximum down to 800 m depth at station 12, as do CFC data discussed in the paper of *Forner* [2005], at the offshore edge of the EGC. It could possibly be related to locally convected water but has θ-*S* characteristics of upper Labrador Sea Water (uLSW, see Figure 11). Another O_2 maximum characteristic of the classical Labrador Sea Water (cLSW) lies at about 1500 m. Upper LSW is also seen in an anticyclonic eddy at station 20, embedded in saltier and less oxygenated water influenced by the North Atlantic Central Water.

[45] A question is to determine how the Irminger cyclonic circulation is embedded into a larger circulation scheme. Connections between the Irminger gyre and the NAC over the Reykjanes Ridge (RR) were suggested by surface drifters [*Krauss*, 1995; *Flatau et al.*, 2003] and at intermediate depth by floats [*Lavender et al.*, 2000]. On the Ovide section, the θ-*S*-O_2 properties in the east Irminger Sea show a strong mesoscale variability and a significant interleaving. The connection with the NAC is observed but not straight through the RR. Indeed, the subarctic front, which delimits the eastern subpolar gyre at stations 48–53, is also intersected twice in the vicinity of the RR: at stations 23–25 and stations 35–37 (Figure 2). The absolute dynamic topography measured by satellite altimetry (Figure 12) consistently suggests an anticyclonic surface circulation around RR. This anticyclonic circulation encompasses a pool of subpo-

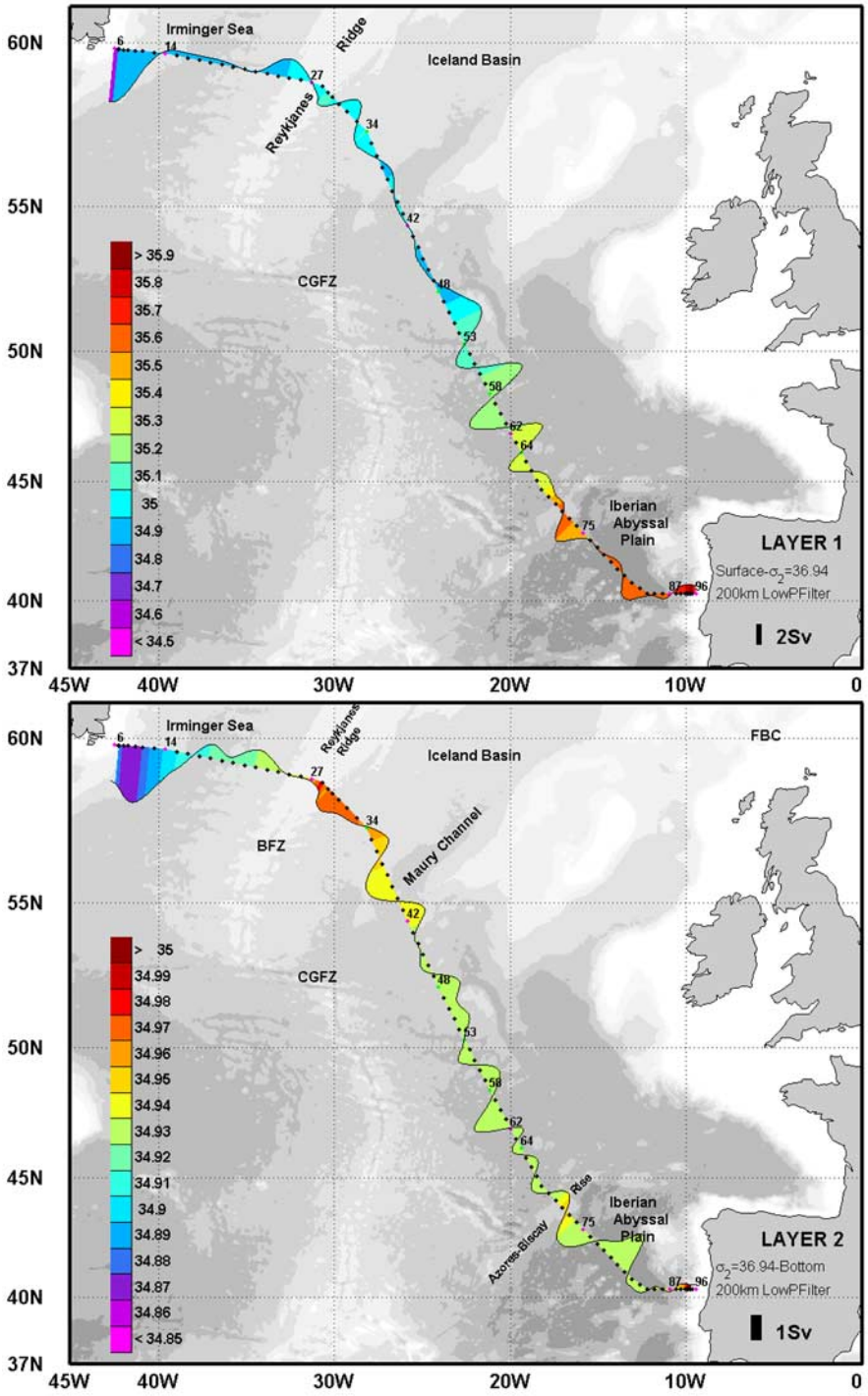

Figure 9. Same as Figure 7 but for layers between the surface and σ_2 = 36.94 (top) and between σ_2 = 36.94 and bottom (bottom). Transports have been low-pass filtered with a cutoff wavelength of 200 km to enhance large-scale patterns.

lar mode water that is identified around station 33 by its homogeneity and its salinity greater than 35 (Figure 2). The larger thickness of the mode water is within the already mentioned anticyclonic eddy centered at station 33. The eddy core, found at 500 m depth (Figure 4), has no clear surface expression (Figure 12).

[46] The main branch of the North Atlantic Current is found at 52°N (stations 48–51, Figures 8 and 9a), 50 km south of the latitude of the Charlie Gibbs Fracture Zone (CGFZ), which marks the northernmost limit of this NAC branch [*Sy*, 1988; *Belkin and Levitus*, 1996; *Schott et al.*, 1999]. A second branch, less intense, is observed at stations 62–63. Eddies are embedded between these two branches (Figures 9a and 12). We estimate 21 ± 2 Sv for the transport of the NAC between 52°N and 45°30′N (Figure 10, first layer between stations 42 and 66), a value that is weaker

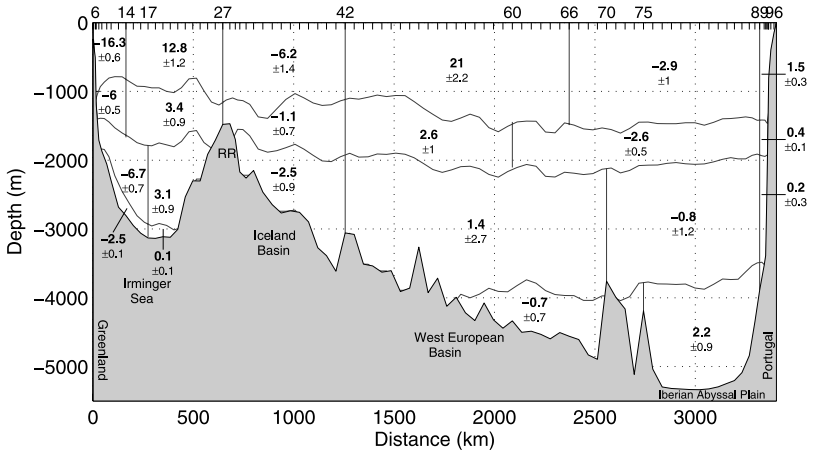

Figure 10. Transports in Sv crossing the Ovide section in 2002 (*S*-sadcp solution), integrated over boxes. The errors are given by the model after inversion. Layer limits are $\sigma_1 = 32.35$, $\sigma_2 = 36.94$, and $\sigma_4 = 45.85$.

than some estimates (about 35 Sv between 40° and 54°N in the work of *Cunningham* [2000] and *Paillet and Mercier* [1997]) but consistent with the 19 Sv at 52°N in the study of *Bacon* [1997].

[47] South of the 44°N meddy already mentioned in the previous section (station 71), a southward net transport can be identified in Figure 8. This southward circulation in the Iberian basin has been documented by *Paillet and Mercier* [1997] and amounts to 3 ± 1 Sv in the NAC layer ($\sigma_1 <$

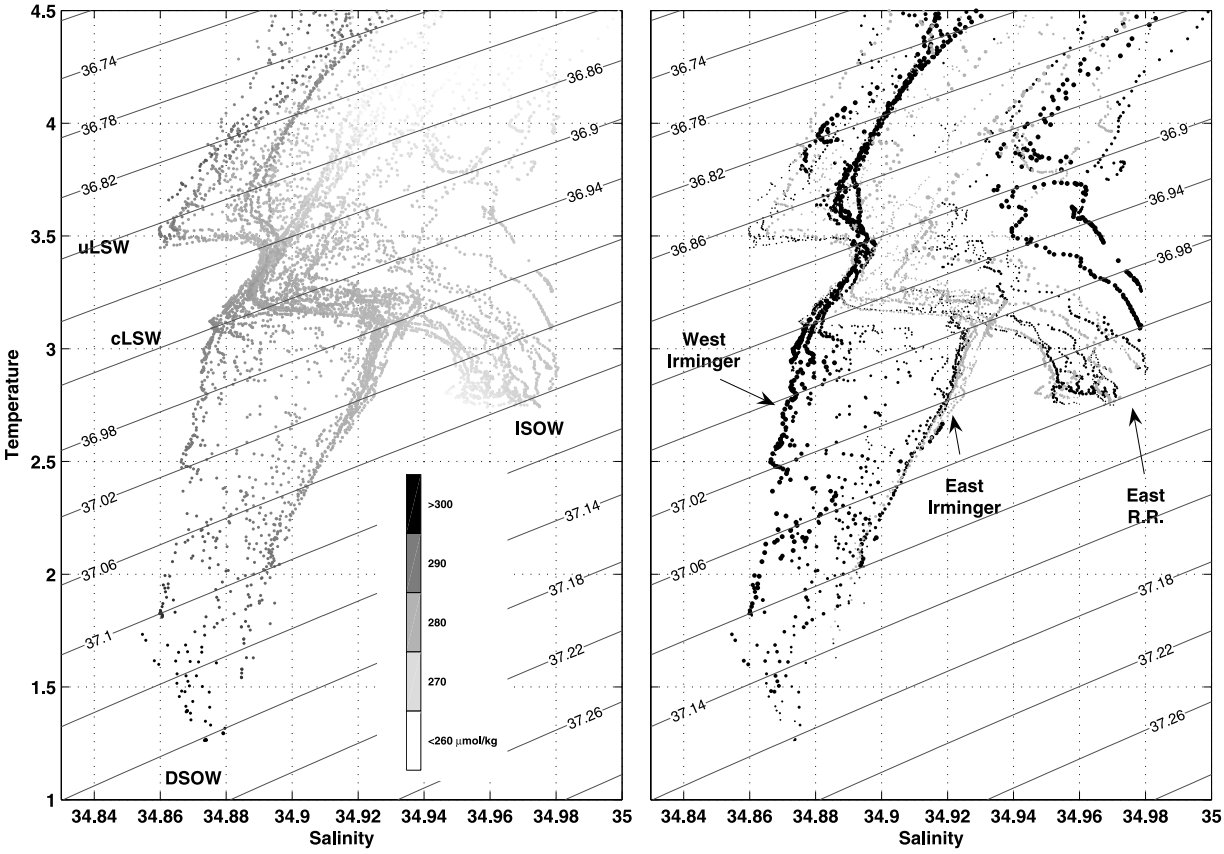

Figure 11. θ-S diagrams of stations 6 to 42. Properties have been averaged in 10-m layers for each pair of stations. On the left diagram, each point is colored according to its oxygen value. On the right diagram, black (grey) points figure southwestward (northeastward) velocities in the model, respectively, and large dots indicate velocities greater than 0.1 m s^{-1}.

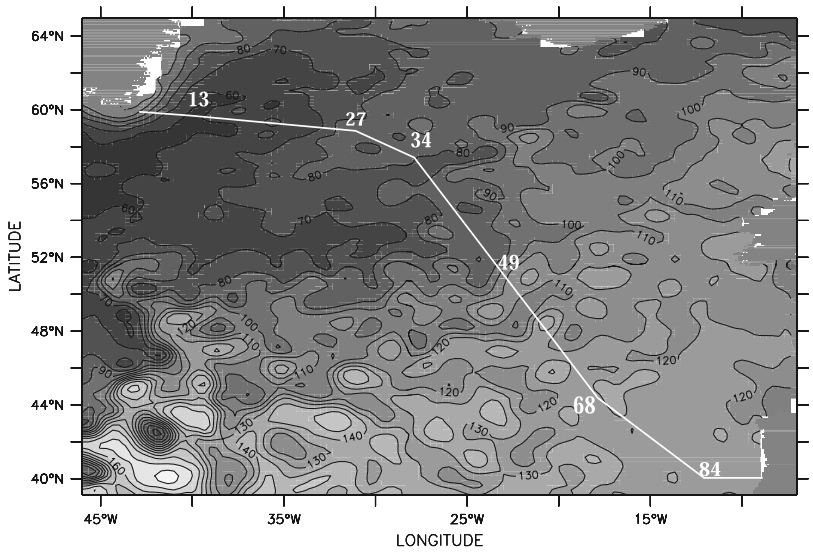

Figure 12. Merged absolute dynamic topography in centimeter calculated for 26 June 2002 (from the AVISO Live Access Server). The Ovide track is superimposed in white.

32.35) in 2002. It is of particular importance for the southward advection and subduction of the eastern North Atlantic Mode Water formed in the deep winter mixed layer to the north of the Ovide section.

[48] A net warm water transport of 19 Sv across a zonal section at 52°N was found in 1991 by *Bacon* [1997], and it can be compared to the net 19.6 Sv crossing the Ovide section in June 2002 east of 27°W (stations 42 to 96, Table 3).

4.3. Lower-Layer Circulation ($\sigma_2 < 36.94$)

[49] The Iceland-Scotland and Denmark Strait overflows are the two sources of the North Atlantic Deep Water coming from the Nordic seas. The Ovide line intersected the DWBC transporting the Iceland-Scotland Overflow Water (ISOW) on the eastern side of the RR upstream of the Charlie Gibbs Fracture Zone (CGFZ). This branch transports 2.5 Sv southward (Figure 10, Table 3), similar to the mean transport value reported by *Saunders* [1994] in the CGFZ for $\sigma_0 > 27.8$. From Figure 9b, two peaks of southward flow can be observed: one on the slope of RR, associated with a maximum of temperature and salinity (Figure 2), and a deeper one, partly associated with a deep cyclonic circulation in Maury Channel [*Harvey and Theodorou*, 1986]. The properties of both branches can be seen in Figure 11: They constitute the saltier deep water of the θ-S diagram, lying from $S = 34.95$, $\theta = 2.76$°C for the deeper (eastern) branch, to $S = 34.975$, $\theta = 3.25$°C for the slope branch, richer in oxygen. In the deeper branch, we also observe a relative maximum in the amount of silicate (greater than 15 μmol kg^{-1}; P. Morin, personal communication). Therefore from the analysis of its hydrological properties and from the deep circulation scheme shown by *Schmitz and McCartney* [1993] (their Figure 12), we conclude that the water of the deep branch transports ISOW from the Faroe-Bank Channel and undergoes the influence of upwelled AABW circulating cyclonically around the northeast Atlantic. This data set does not bring clues on the origin of the upper branch: According to *Harvey and Theodorou* [1986] or *van Aken and Becker* [1996], it could come from the sills west of Faroe Islands as well as from the Faroe-Bank Channel.

[50] In the eastern half of the Irminger Sea, the deep northward flow found between stations 17 and 27 (Figure 9b) amounts to 3.2 Sv (Figure 10, Table 3). The core of this flow is made of ISOW and classical Labrador Sea Water (cLSW), forming a distinct elbow at $\theta = 3.1$–3.25°C and $S = 34.92$–34.93 in Figure 11b, with northward (grey) velocities. The deep cyclonic circulation in the Irminger Sea is revealed by the θ-S characteristics of its eastern limb which is influenced by Denmark Strait Overflow Water (DSOW, Figure 11a). Estimating the amount of recirculating DSOW is difficult since the errors on the flows west of RR add up to 1 Sv. Furthermore, we found that 80% of the additional 0.7 Sv flowing northward west of RR (as compared to east of RR in Figure 10) lays between $\sigma_2 = 36.94$ and $\sigma_2 = 36.98$, i.e., in the cLSW layer, and we would need a careful tracer analysis to separate the recirculating LSW from the directly imported one (along the path shown in the work of *Lavender et al.* [2000]).

[51] The DWBC off Greenland transports 9.2 ± 0.9 Sv (Figure 10, Table 3), and it mainly lies between 1700 and 2900 m, with an intense barotropic flow inshore of the 2000-m isobath and a more moderate and mainly baroclinic flow offshore. Although the position of the current is consistent with observations in 1987–1990 reported by *Dickson and Brown* [1994], its transport is weaker than the 13 Sv previously estimated at Cape Farewell. One might object that we are dealing with a snapshot in an area of strong variability at a scale of a few days, as underlined by mooring measurements of *Dickson and Brown* [1994]. However, in mooring estimates, part of this variability may be spatial and not temporal, and the integration performed by our geostrophic estimates might smooth out this part. Furthermore, the interannual variability of the DWBC transport was consistently documented by *Bacon* [1998a] from hydrographic sections. For comparison with this latter work, we split our DWBC transport into a

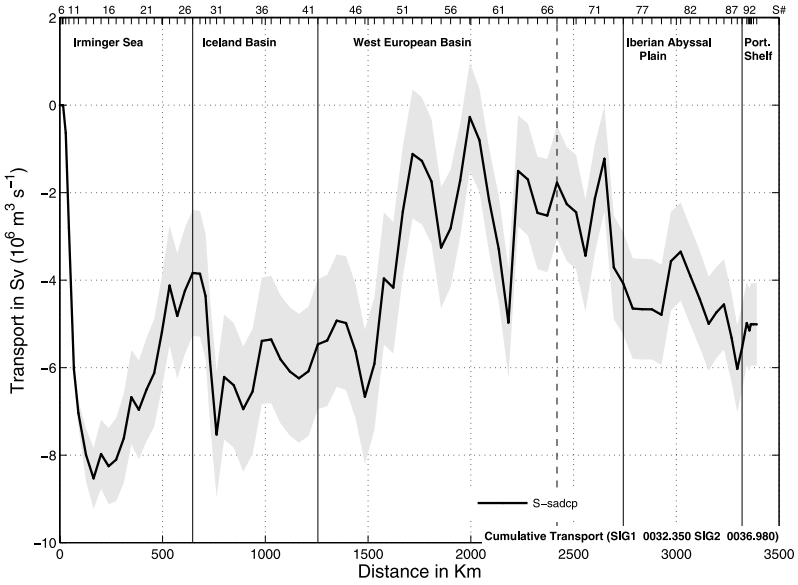

Figure 13. Cumulative transport from Greenland (left) to Portugal (right), vertically integrated between σ_1 = 32.35 and σ_2 = 36.98 (see Figure 2) and plotted against distance along the Ovide section (as in Figure 8). Station numbers labeled at the top of the plot.

baroclinic contribution (5.2 Sv) and a reference level velocity contribution (4 Sv). The baroclinic contribution to the DWBC observed during Ovide is similar to the values reported by *Bacon* [1998a] for the late 1990s (4–5 Sv). During the 1980s, the DWBC transport was larger by about 3 Sv.

[52] The relative contribution of DSOW in the 60°N DWBC can be evaluated in Ovide since no deep sill exists between Iceland and 58°N, where the section crosses the RR: All the ISOW and LSW must cross the section northward west of the ridge (3.2 ± 1.0 Sv, Figure 10) before recirculating in the 9.2-Sv DWBC. So we obtain an estimate of 5–7 Sv for the transport of DSOW, which includes entrainment between Denmark Strait and 60°N.

[53] The deep circulation in the West European Basin is mainly influenced by the spreading of the Labrador Sea Water [*Paillet et al.*, 1998]. The volume transport integrated between σ_1 = 32.35 and σ_2 = 36.98 and accumulated from Greenland to Portugal is shown in Figure 13. According to Figure 2, this plot is representative of LSW transport between the RR (station 27) and 45°N (station 67). About 4 Sv of LSW is found to cross the section northward under the main branch of the NAC, between 51°30′ and 52°30′N, while about 2 Sv flows southward above ISOW east of the RR. This implies a net export of 2 ± 1 Sv toward the Iceland Basin, as found in the paper of *Bacon* [1997]. In the eastern Irminger Sea, two additional Sverdrups come from the southwest (the Labrador Sea and the Irminger cyclonic gyre), as discussed earlier, while about 4 Sv of uLSW (or Irminger Sea Water) is exported above the DWBC.

[54] We know from the study of *Paillet et al.* [1998] that due to its orientation, the section may intersect a meander of the southeastward spreading of the LSW, with a weak signature in the transports perpendicular to the section. In the data, the southwestward flow that is supposed to underline the southern limit of the LSW influence is not clearly observed due to the predominance of the mesoscale circulation.

[55] In the Iberian Abyssal Plain, a net northward flow transports 2.2 Sv of Antarctic Bottom Water and Lower Deep Water (Figure 9b, stations 75 to 89). One third of this deep flow recirculates cyclonically north of the Azores Biscay Rise (stations 54 to 70), while two thirds is upwelled in the Lower Deep Water.

5. Fourex 1997 Revisited With ADCP Data

5.1. Presentation of the Fourex Reanalysis With ADCP Data

[56] The Fourex section (Figure 1) has already been analyzed and interpreted in terms of physical and biogeochemical transports by *Àlvarez et al.* [2004] (hereafter referenced to as A04). Current measurements from 150 kHz SADCP and LADCP were not used, and the velocity at the reference levels was deduced from average numbers found in the literature. Now using the direct current measurements [*Bacon*, 1998b], the calculation of the transports can benefit from synoptic current values. So the objective is to apply exactly the method, described in section 3, without climatological constraints.

[57] As our inverse model is slightly different from the one used in A04 (described in the paper of *Àlvarez et al.* [2002]), a first step was to run the model using the exact constraints described by A04. These constraints consist of a 25 ± 1 Sv total southward flow from Greenland to 110 km offshore (EGC), a 2.4 ± 1 Sv southward deep flow in the CGFZ, no net transport of AABW (±2 Sv), and a salt conservation ($\pm 35 \times 10^9$ kg s^{-1}). The resulting transports of both models all lay within the respective errors, and we could then proceed to include ADCP data plus overall mass conservation (±3 Sv) instead of constraints described above.

[58] As explained earlier, SADCP data are more appropriate than LADCP data for bringing information at each

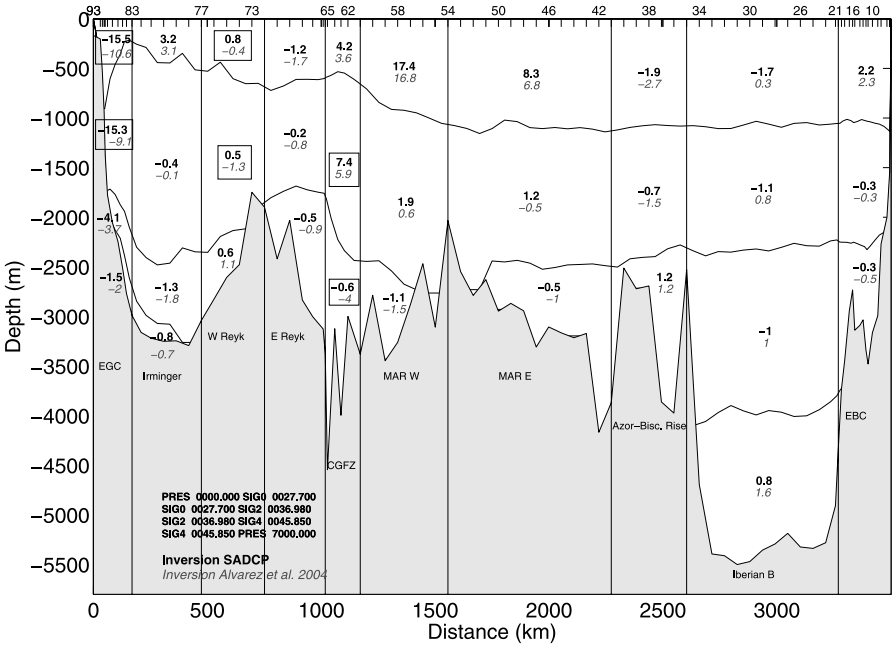

Figure 14. Transports across Fourex section (Sv), positive northward. Layer limits are σ_0 = 27.7, σ_2 = 36.98, and σ_4 = 45.85. Faint italic numbers are from the work of *Àlvarez et al.* [2004]. Bold numbers are for the new inversion with SADCP data from Greenland to station 46 (at 2000 km). Large differences between both inversions are surrounded with a box.

pair of stations. However, they were found too much noisy in the southeast part of the section, and unfortunately, the LADCP data are also lacking in the same area. Knowing that in this part of the section, transports can be reasonably deduced from geostrophy provided that the reference level is properly chosen, we used SADCP data on 48 pairs of stations (2000 km) from Greenland to station 46 at 45°47′N–24°39′W. Reference levels were chosen, as in A04, apart from the following pairs: In CGFZ, the reference levels for pairs 62–63 and 64–65 were raised to 3000 and 2500 m, respectively, to match the shallower level of the topography between the stations and be consistent with the LADCP-measured level of no motion.

[59] SADCP data were given with no variance for each averaged profile on 600-m route segments. Relying on Ovide statistical analysis on segments of similar length, we apply a 30 cm s^{-1} standard deviation to the Fourex SADCP velocities, and from there, transport errors between 32 and 200 m (or bottom) are calculated as explained in subsection 3.5.

5.2. Results

[60] A comparison between the A04 results and the new inversion of Fourex data is shown in Figure 14. Limits in density are those chosen in A04: four layers separated by σ_0 = 27.7, σ_2 = 36.98, and σ_4 = 45.85. Main differences are summarized in Table 2. The North Atlantic Current intensity has not significantly changed: We find that the A04 value of +27.1 Sv is increased to +28.5 Sv, but these values are found within the errors of the inverse model. We see also that the DWBC along the Greenland slope has not significantly changed either. This current includes the DSOW and part of the ISOW that has circulated in the Irminger Basin.

[61] The two main differences are seen in the East Greenland Current and in the deep flow around CGFZ. Direct current measurements all show a much stronger current in the western boundary of the section. The SADCP constraints lead to an EGC that is 11 Sv more intense than in A04. The LADCP confirms this result, with a 37 Sv southward flow on the whole water column (to be compared with the 36.4 Sv summed over the left boxes of Figure 14 and with the 25 Sv imposed in A04). We conclude that this particular constraint was too low in A04.

[62] The 2.2 ± 0.7 Sv southwestward bottom flux in the CGFZ area below σ_2 = 36.98 is three times weaker in the new results, and most of the difference is found within the five station pairs of CGFZ itself. The new result is more consistent with direct current measurements and is also consistent with simultaneous observations of *Schott et al.* [1999]. The flow calculated below the usual σ_2 = 36.94 (σ_0 = 27.8) gives only 1.2 Sv westward, but it includes some eastward flowing LSW, which is once again in agreement with the study of *Schott et al.* [1999]. It can theoretically be compared to the annual average of 2.4 ± 0.5 Sv calculated by *Saunders* [1994] below σ_0 = 27.8. However, this comparison is misleading if one wants to look at the ISOW

Table 2. Comparison of Transports Between Fourex Inversions in the Main Currents (Positive Northward), Summarized From Figure 14[a]

Region	Layer	Stations	A04, Sv	ADCP, Sv
EGC	$\sigma_2 < 36.98$	83–93	−19.7 ± 0.8	−30.8 ± 0.7
CGFZ	$\sigma_2 > 36.98$	54–72	−6.4 ± 1.4	−2.2 ± 0.7
DWBC	$\sigma_2 > 36.98$	77–93	−8.2 ± 0.9	−7.7 ± 0.7
NAC	$\sigma_0 < 27.7$	3–65	+27.1 ± 1.9	+28.5 ± 1.3

[a]Errors are estimated by the inverse model.

Table 3. 2002 Transports in the Main Currents of the North Atlantic (Positive Northward)[a]

Region	Ovide Stations	Transport, Sv
EGC	6–14	−22.4 ± 1.1
DWBC	6–17	−9.2 ± 0.9
DSOW	6–17	−6.0 ± 1.3
RR-E DBC	17–27	+3.2 ± 1.0
RR-W DBC	27–42	−2.5 ± 0.9
NAC (net)	42–96	+19.6 ± 1.7

[a]Errors are estimated by the inverse model. The East Greenland Current (EGC) is defined here with $\sigma_2 < 36.94$ (equivalent to $\sigma_0 < 27.8$). DWBC stands for deep western boundary current (off Greenland), DBC for deep boundary current, RR-E and RR-W for the Reykjanes Ridge-East and Reykjanes Ridge-West, respectively, and DSOW for Denmark Strait Overflow Water. All the deep transports (DWBC, DSOW, and DBC) are calculated using $\sigma_2 > 36.94$. The North Atlantic Current (NAC) is defined with $\sigma_1 < 32.35$.

southward flow. Indeed, records in central Labrador Sea show a maximum of LSW volume and density between 1990 and 1994 (I. Yashayaev and A. Clarke, unpublished manuscript, 2005, Figure 2), 0.08 kg m^{-3} denser than in the mid-1980s. By 1997, this water has spread over CGFZ, replacing part of the ISOW. So the 2.2 Sv southwestward flow measured in CGFZ below σ_2 = 36.98 is a more appropriate value for ISOW transport.

[63] *Schott et al.* [1999] suggest also that the deep flow variability in CGFZ may very well be correlated with the NAC position by modifying the barotropic northeastward flow in the area. In the Fourex case, this idea is actually supported by the evidence of a strong surface northward flow, which is found above and southeast of CGFZ. However, surface hydrological properties are not typical of the NAC. It is possible also that there is some variability in the proportion of ISOW entering the Irminger Basin north of CGFZ through the 2000-m deep Bight Fracture Zone at 57°N or the 2400-m sill at 55°N.

[64] Figure 9 of A04 shows that ISOW is the major water mass found between stations 54 and 72, and this 2.2 Sv will most likely contribute to the DWBC. The 0.6 Sv found west of RR is mainly ISOW circulating in the Irminger Sea. Thus 1.6 Sv may feed the DWBC south of Fourex.

[65] At 60°N, the DWBC is 9.3 ± 1.1 Sv below σ_2 = 36.98. Calculated below σ_2 = 36.94, it sums up to 11.3 ± 1.2 Sv southward.

[66] Finally, it may be noted that the new inversion leads to a slight increase of the northward flow of Labrador Sea Water in the Eastern Basin.

6. Comparison Between 1997 and 2002

6.1. Regional Differences

[67] Ovide 2002 and new Fourex 1997 transports can now be compared (Tables 3 and 5). Because of the different path followed by the two experiments, several difficulties arise in this task.

[68] The DWBC (off Greenland) shows a 2.1-Sv decrease (i.e., about 20%) between August 1997 and June 2002. The relative contribution of LSW, ISOW, and DSOW cannot be known in Fourex without a careful analysis of the different properties (as done in A04 with the Optimum Multiparameter approach), and this is beyond the scope of this paper. As discussed in subsection 4.3, it is however possible to separate the contributions of the DSOW and of the other deep waters (ISOW and cLSW) in the Ovide DWBC, as summarized in Table 3.

[69] The NAC can only be compared when calculated globally from the subarctic front (SAF) to the Iberian Coast. Although very crude, this estimate takes better account of the robustness of inverse models regarding the large-scale patterns. For both 1997 and 2002, the subsurface horizontal gradient of temperature has been chosen to localize the SAF. The 30% decrease of the warm water transport northward between 1997 and 2002 is striking and cannot be caused by the different station location. Alarming papers on the subject have already been published [*Bryden et al.*, 2005], but *Treguier et al.* [2006] show that the NAC variability found along Fourex can also be seen in the models and may very well be due to monthly to interannual variability. This open question may be tackled in a later paper using altimetry data with past and future hydrographic sections (including repeat Ovide surveys).

[70] The EGC variability (27.7 Sv in 1997 versus 22.4 Sv in 2002) is also documented by *Treguier et al.* [2006], with a quite surprising match between the CLIPPER model and the data. It is found to be consistent with the weakening intensity of the subpolar gyre shown by *Häkkinen and Rhines* [2004].

6.2. Volume Transport as a Function of Depth

[71] The net volume transport associated with the large-scale circulation across the section can be calculated in depth coordinates (Figure 15). The MOC strength (MOC_z) is most often calculated as the transport of North Atlantic Deep Water (NADW) [*Marsh et al.*, 2005; *Àlvarez et al.*, 2004]. It is represented by the surface of the shaded areas between the two zero crossings at about 1000 and 3500 m. The important differences seen between 1997 and 2002 values (14.2 versus 11.2 Sv, Table 4) come with significant differences in the shape of the horizontally integrated transport in Figure 15.

[72] The northward flow observed above 1300 m is mainly the algebraic sum of the NAC and the EGC. In this layer, we observe that the net transport cancels at a much deeper depth in Fourex (1250 m) than in Ovide (950 m). Inspection of the average depth of the σ_1 = 32.35 isopycnal and of the velocity fields shows that the NAC depth extension is equivalent in Ovide and in Fourex and cannot explain the different depths of the zero crossing nor the different amplitude of the transport above it in Figure 15. The NAC is 7 Sv stronger in 1997 (Table 5), and is the main factor in the intensification of the northward flow above 1300 m, although the net result is moderated by the opposite EGC variability as seen in Tables 3 and 5.

[73] Since we observed that the NAC vertical extension is similar in depth for both years, we conclude that the difference in depth of the zero crossing is mainly driven by the northeastward transport of LSW which is particularly intense between 1000 and 2000 m depths above CGFZ in 1997. Knowing that LSW takes 2 to 6 years to spread over the Mid–Atlantic Ridge, the 1990–1994 anomaly mentioned in subsection 5.2 is likely to create the observed northward transport anomaly above the MAR at LSW depth. This transport is partly compensated in the net

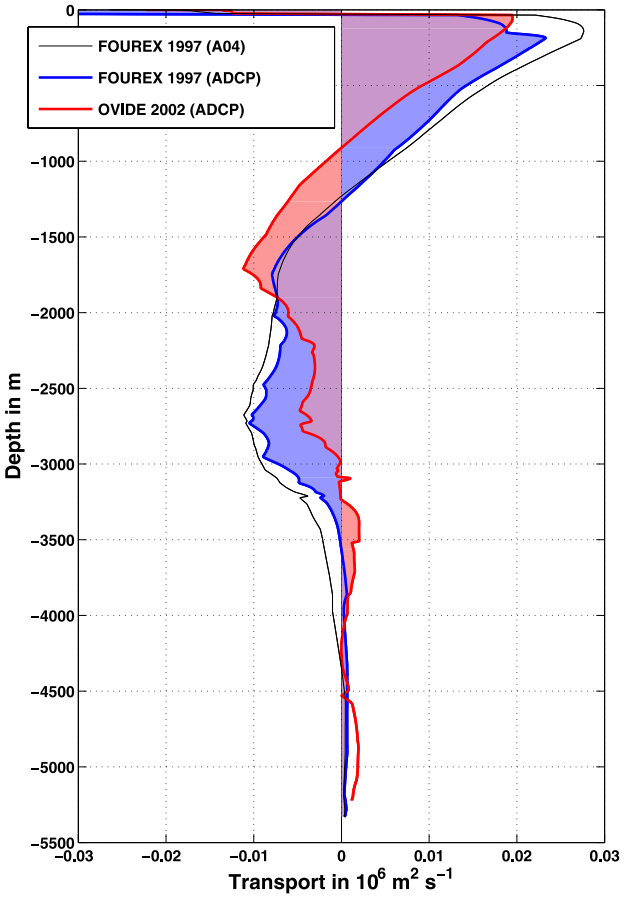

Figure 15. Transport integrated over the whole section with a 1 m vertical resolution. The result of Fourex 1997 from the study of *Àlvarez et al.* [2004] inversion is the thin black line. The thick blue line is from the 1997 ADCP solution, and the thick red line is from the Ovide 2002 ADCP solution. For both lines, the surface of the shaded area underneath gives the net transport in both directions.

balance by the export of uLSW (or Irminger Sea Water, as suggested by A04 following the work of *Pickart et al.* [2003]) at the bottom of the EGC. However, between 1400 and 2500 m, this LSW transport anomaly definitely weakens the net southwestward transport in Figure 15.

Table 4. Comparison Between 1997 and 2002 Integrated Transports[a]

	1997_{ADCP}	$2002_{S\text{-}sadcp}$	Units
MOC_z/NAC	13.2 ± 0.9	8.8 ± 0.9	10^6 m^3 s^{-1}
MOC_z/NADW	14.2 ± 0.8	11.2 ± 0.8	10^6 m^3 s^{-1}
MOC_σ	19.2 ± 0.8	16.9 ± 1.0	10^6 m^3 s^{-1}
Net Transp.	0.12	0.26	10^6 m^3 s^{-1}
Heat	0.66 ± 0.04	0.44 ± 0.05	10^{15} W
Salinity	15.2 ± 4.3	8.2 ± 4.4	10^9 kg s^{-1}

[a]The MOC is calculated in z coordinates as the maximum of the transport accumulated over the whole section from surface to bottom (the shallower shaded area in Figure 15) and as the difference of its extrema (the intermediate shaded area in Figure 15). The MOC_σ is calculated as the maximum of the cumulative transport but in σ coordinates (Figure 16). "Net Transp." refers to the net volume transport in the inverse model. Errors are given by the inverse models and do not take into account sources of errors like the asynopticity and the ageostrophic variability along the section but include EGCC sampling error (see subsection 4.1).

Table 5. 1997 Transports in the Main Currents of the North Atlantic With the Same Conventions as Table 3

Region	Fourex Stations	Transport, Sv
EGC	83–93	−27.7 ± 0.6
DWBC	77–93	−11.3 ± 1.2
NAC	03–61	+26.6 ± 1.6

[74] The southward flow between 1300 and 3000 m (3500 m in 1997) is mainly formed by the DWBC off Greenland and is influenced by the currents in CGFZ (in 1997) and along RR (in 2002). It extends deeper in Fourex mainly because the DWBC is crossed deeper, about 200 km further south, and is more intense in 1997, creating a prevalent feature in the bottom part of the southward transport.

[75] Below 3500 m, both inversions show a net northward flow of AABW that forms the eastern branch of the deep cyclonic circulation, the western branch being shallower [*Schmitz and McCartney*, 1993]. The AABW northward flow below 3800 m in Fourex transports is weaker than in Ovide (0.8 against 1.5 Sv, Figures 10 and 14), but the associated errors prevent us from interpreting this as a temporal variability.

6.3. Volume Transport as a Function of Density

[76] By meridional overturning cell, we want to refer to the vertical cell composed on the one hand by the North Atlantic Current that feeds the subpolar seas with warm water and on the other hand by the deep western boundary current that brings the overflow waters and the recirculating Labrador Sea Water southward.

[77] We conclude from the previous section that integrating the shaded surfaces of Figure 15 to obtain an estimate (MOC_z) of the MOC is not totally satisfying. Indeed, any slight variation of some horizontal circulation patterns, mainly the EGC, the northward bottom current, and the spreading of the LSW, are modifying the value of MOC_z. That is why, the transport integrated in layers of 0.1 kg m^{-3} (in σ coordinates) is now examined (Figure 16). Once again, an indication of the circulation strength is given by the surface of the shaded areas. The surface above the zero crossing corresponds to the maximum cumulative transport northward and defines the thermohaline circulation (THC) strength according to *Marsh et al.* [2005]. For clarity, we prefer to call it MOC_σ, and we find 19.2 Sv in 1997 as compared with 16.9 Sv in 2002 (Table 4).

[78] The zero crossing of Figure 16 occurs for $\sigma_1 = 32.1$ both in 1997 and in 2002. It can be seen from Figure 4 that the $\sigma_1 = 32.1$ isopycnal nearly surfaces above the EGC, and the northward transport in the MOC_σ mostly includes the NAC. Thus MOC_σ is representative of the water mass transformation occurring north of the section.

[79] We notice that MOC_σ is stronger than the DWBC by about 7.5 Sv for both years. This difference can be explained by the export of some EGC water (mainly Irminger Sea Water and uLSW) from the Irminger Sea. Part of this water circulates cyclonically around the Labrador Sea before merging with the Labrador Current; a significant part enters the Labrador Sea (via eddies) and is transformed by isopycnal mixing or incorporated in the process of LSW formation. The fact that Ovide and Fourex MOC_σ values are so close to the MOC_z values at lower latitudes [*Koltermann*

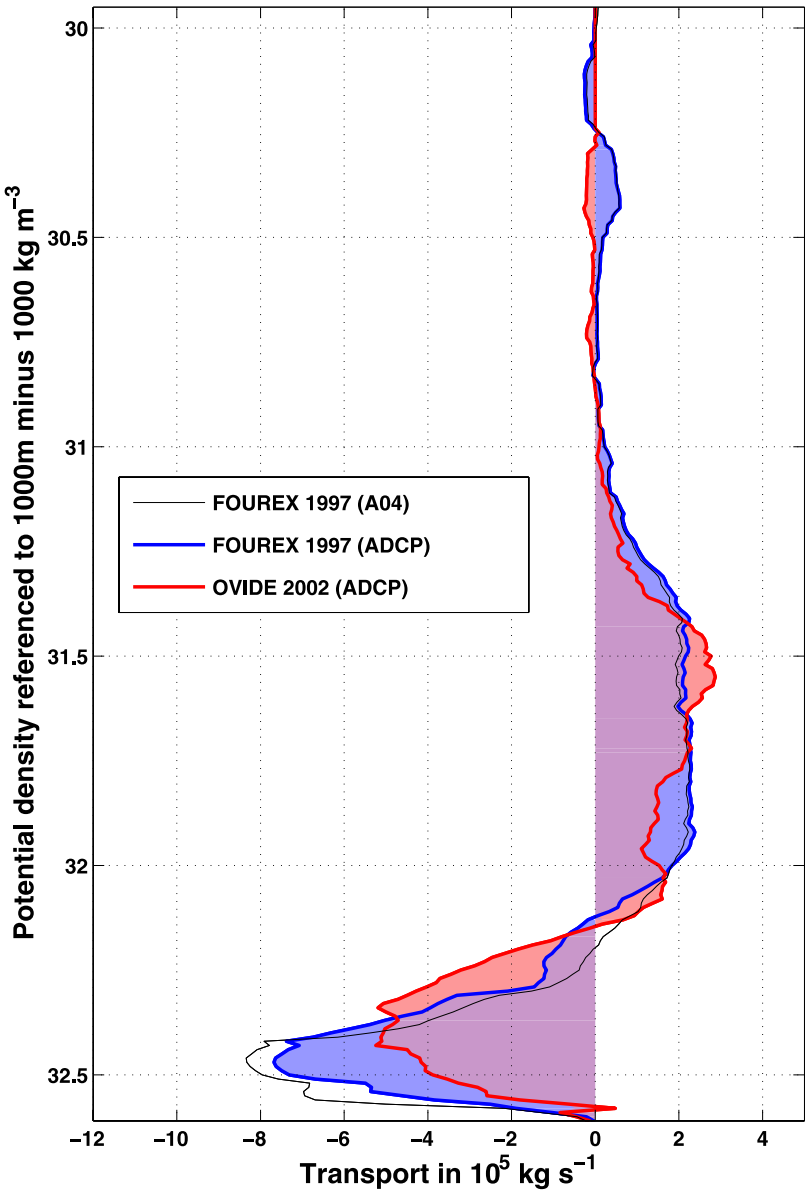

Figure 16. Same as Figure 15 in density layers, with a 0.01 kg m^{-3} vertical resolution. Values are in 10^5 kg s^{-1}.

et al., 1999; *Bryden et al.*, 2005] leads us to believe that the EGC water exported westward with a density above σ_1 = 32.1 belongs to the lower branch of the MOC at lower latitudes either by deepening of the isopycnals south of the Labrador Gyre or by diapycnal mixing inside the gyre. Future studies will help to validate and develop this thesis.

6.4. MOC Strength and Heat and Freshwater Transports

[80] By performing different inversions, using or not LADCP and/or SADCP, and applying various constraints, we found that the MOC$_z$ was actually quite sensitive to changes in the constraints, whereas the MOC$_\sigma$ was much more stable. For example, MOC$_z$ varies from 17 to 14.2 Sv between the A04 and the 1997 ADCP inversion, while MOC$_\sigma$ varies only from 19 to 19.2 Sv. Similarly, comparing *S*-sadcp and *S*-geost inversion in 2002 (with and without ADCP data), MOC$_z$ differs by 4.3 Sv while MOC$_\sigma$ differs by only 0.1 Sv.

[81] Table 4 gives a summary of the different values for estimates of MOC strength and for heat and salt transports. The error is a result of the inversion, and in 2002, 0.7 Sv associated with the EGCC has been incorporated (see subsection 4.1).

[82] Values of 14.2 Sv in 1997 and 11.2 Sv in 2002 are obtained for MOC$_z$/NADW in Table 4; however, the MOC$_z$/NAC strength calculated as the peak in the transport accumulated from the surface represents 13.2 and 8.8 Sv, respectively. Why are MOC$_z$/NADW and MOC$_z$/NAC so different? We observe a 2002 AABW net transport of 1.5 ± 1.1 Sv northward, twice as strong as in 1997 according to the new ADCP inversion. This strong flow participates in the difference between the two MOC definitions through the overall mass conservation and is associated with the trans-

formation of upwelled AABW in NADW north of the section.

[83] This discussion leads us to consider that the MOC strength calculated in σ coordinates is a better proxy for the MOC than the estimates calculated over z coordinates, as stated by *Marsh et al.* [2005]. With uncertainties based on one-standard-deviation range, we find that the MOC amplitude in June–July 2002 was significantly lower than in August 1997, with a decrease of 2.4 ± 1.8 Sv (about 15%). The maximum of the northward transport was obtained at σ_1 = 32.1, which lies at about 1000 m within the NAC.

[84] The heat transport is equal to 0.44 ± 0.05 PW (1 PW = 10^{15} W) in 2002, while it reached 0.66 ± 0.04 PW in 1997, which corresponds to a difference of about 30%.

[85] The salinity flux is calculated, assuming a strict zero mass flux as in the work of *Bacon* [1997], obtained by imposing a mass conservation error of 0.1 10^9 kg s^{-1}. We find 8.2 ± 4.4 Sv psu northward in 2002 against 15.2 ± 4.3 Sv psu in 1997 (Table 4). The errors include the possible omission of 0.7 Sv at 31 psu in the EGCC in 2002. The variability, although not significant, is consistent with the heat flux, reminding that the NAC is the main heat and salt source across the section. The Ovide 2002 value is similar to Bacon's 6.5 ± 2.2 Sv psu in 1991.

7. Discussion and Conclusion

[86] The question arises whether the slightly different paths and seasons of Fourex and Ovide could explain some of the observed variabilities in the MOC strength. Although many qualitative issues were discussed in subsection 6.2, the net impact of the observed differences is difficult to quantify without the help of models. That is why, this issue was thoroughly discussed in the paper of *Treguier et al.* [2006] using the eddy-resolving CLIPPER ATL6 and FLAME models for the 1995–2002 period. The models consistently show larger values of MOC_σ by 1–2 Sv across Fourex line than Ovide in all seasons, whereas the models present a 2- to 4-Sv decrease between Fourex 1997 and Ovide 2002. This is quite consistent with the data and suggests that the observed difference in MOC_σ is mostly time variability and not space variability. The differences are enhanced in depth coordinates, but they may also be less reliable, as discussed before.

[87] *Treguier et al.* [2006] also showed that the orientation of the section allowed us to safely ignore the unresolved eddy contribution to the heat transport across the Ovide section. The difference in heat transport is remarkable (0.66 PW in August 1997 versus 0.44 PW in June 2002), but there again, the southern localization of the Fourex line could be partly responsible since the sections, although not zonal, lie on the steep slope of the zonally averaged heat transport [see the work of *Ganachaud and Wunsch*, 2003, Figure 3]. To verify this potential contribution, the yearly averaged surface heat flux between Ovide and Fourex sections was estimated as 0.02 PW, which indicates that the different paths of the sections are not responsible for the observed difference in heat transport. What about the monthly variability? The CLIPPER model run from the paper of *Treguier et al.* [2006] shows that the heat transport across Ovide section has the smallest variability in summer, and the difference estimated between June and August averaged on years 1995 to 2002 in the model gives −0.02 PW, with a standard deviation of 0.05 PW. On the basis of these model results, the difference in time and location of Ovide and Fourex sections would explain at most one third of the contrast observed between 1997 and 2002. This suggests that the observed heat transport variability is mainly a direct result of the MOC_σ variability between August 1997 and June–July 2002.

[88] What about nonsynopticity issues? The Ovide section was performed in 22 days. According to *Ganachaud* [2003], the uncertainty linked to the asynopticity is weak compared to those associated with geostrophic assumptions. Although these sources of error were included in the overall mass constraint, it has little effect on the resulting MOC error since the constraints from velocity measurements appear to have greater weight. Should we arbitrarily set the resulting MOC error to 3 Sv? We believe we should not; nevertheless, we must emphasize that the present results are only one point representative of 3 weeks of the years 1997 and 2002, and considering the important month-to-month variability of this kind of indicator [*Wunsch and Heimbach*, 2006], conclusions on interannual variability should be drawn with the support of other studies.

[89] In conclusion, it has been shown that the Ovide line is quite suitable to monitor the many circulation patterns of the North Atlantic circulation, including the subpolar gyre, the DWBC, and the NAC. In the eastern subpolar gyre, the circulation is characterized by a strong East Greenland Current of nearly 27.7 Sv in 1997 compared with 22.4 Sv in 2002. In 1997, the northerly boundary of the NAC and the strong northward flow of LSW nearly reverse the flow at depth in CGFZ. In 2002, the NAC net transport is marked by a strong southward recirculation of warm surface water over the Iberian Abyssal Plain, on top of a 2.2 Sv northward flow of AABW.

[90] Besides these circulation patterns, we saw that the maximum of the transport integrated over the section from the surface along σ_1 coordinates is a good proxy for monitoring the North Atlantic meridional overturning cell. Relying on this proxy, we show a 2.4 ± 1.8 Sv decrease in the MOC between summer 1997 and summer 2002, half of it being probably due to the different section paths. The heat transport sees an even more severe decrease of about 30%.

[91] **Acknowledgments.** The authors want to acknowledge the colleagues and ship crews who helped to collect all the data discussed in this paper. They are also grateful to Gilles Reverdin and an anonymous reviewer for their helpful and very detailed comments on the text that helped greatly to improve its precision and clarity. Figure 12 comes directly from the AVISO Live Access Server. For this work, P. Lherminier and C. Kermabon were supported by Ifremer, H. Mercier by CNRS, C. Gourcuff by Ifremer and CNES, and S. Bacon by NOCS. The Ovide project mainly relies on funds from Ifremer, INSU, and PNEDC.

References

Àlvarez, M., H. L. Bryden, F. F. Pérez, A. F. Ríos, and G. Rosón (2002), Physical and biochemical fluxes and net budgets in the subpolar and temperate North Atlantic, *J. Mar. Res.*, *60*, 191–262.

Àlvarez, M., F. F. Pérez, H. L. Bryden, and A. F. Ríos (2004), Physical and biochemical transports structure in the North Atlantic subpolar gyre, *J. Geophys. Res.*, *109*, C03027, doi:10.1029/2003JC002015.

Bacon, S. (1997), Circulation and fluxes in the North Atlantic between Greenland and Ireland, *J. Phys. Oceanogr.*, *27*, 1420–1435.

Bacon, S. (1998a), Decadal variability in the outflow from the Nordic seas to the deep Atlantic Ocean, *Nature*, *394*, 871–874.

Bacon, S. (1998b), RRS DISCOVERY Cruise 230: 07 Aug-17 Sep 1997, *Tech. Rep. 16*, Southampton Oceanography Centre, Southampton.

Bacon, S., G. Reverdin, I. G. Rigor, and H. M. Snaith (2002), A freshwater jet on the east Greenland Shelf, *J. Geophys. Res.*, *107*(C7), 3068, doi:10.1029/2001JC000935.

Bacon, S., W. J. Gould, and Y. Jia (2003), Open-ocean convection in the Irminger Sea, *Geophys. Res. Lett.*, *30*(5), 1246, doi:10.1029/2002GL016271.

Belkin, I. M., and S. Levitus (1996), Temporal variability of the subarctic front near the Charlie-Gibbs Fracture Zone, *J. Geophys. Res.*, *101*(C12), 28,317–28,324, doi:10.1029/96JC02794.

Bersch, M. (2002), North Atlantic Oscillation-induced changes of the upper layer circulation in the northern North Atlantic Ocean, *J. Geophys. Res.*, *107*(C10), 3156, doi:10.1029/2001JC000901.

Billant, A., P. Branellec, and H. Mercier (2004), Campagne OVIDE 2002: Rapport de données CTD-O_2, *Tech. Rep. DRO/DOPS/LPO/04-01*, Ifremer.

Bryden, H. L., H. R. Longworth, and S. A. Cunningham (2005), Atlantic meridional overturning circulation at 25°N, *Nature*, *438*, 655–657, doi:10.1038/nature04385.

Cunningham, S. A. (2000), Circulation and volume flux of the North Atlantic using synoptic hydrographic data in a Bernoulli inverse, *J. Mar. Res.*, *58*, 1–35.

Cuny, J., P. B. Rhines, and R. Kwok (2005), Davis Strait volume, freshwater and heat fluxes, *Deep Sea Res.*, *52*, 519–542.

Curry, R. G., and M. S. McCartney (2001), Ocean gyre circulation changes associated with the North Atlantic Oscillation, *J. Phys. Oceanogr.*, *31*, 3374–3400.

Dickson, R. R., and J. Brown (1994), The production of North Atlantic Deep Water: Sources, rates, and pathways, *J. Geophys. Res.*, *99*(C6), 12,319–12,341.

Dickson, R. R., I. Yashayaev, J. Meincke, B. Turrell, S. Dye, and J. Holfort (2002), Rapid freshening of the deep North Atlantic Ocean over the past four decades, *Nature*, *416*, 832–837.

Egbert, G., A. Bennett, and M. Foreman (1994), TOPEX/Poseidon tides estimated using a global inverse model, *J. Geophys. Res.*, *99*(C12), 24,821–24,852.

Flatau, M. K., L. Talley, and P. P. Niiler (2003), The North Atlantic Oscillation, surface current velocities, and SST changes in the subpolar North Atlantic, *J. Clim.*, *16*, 2355–2369.

Forner, S. (2005), Utilisation des CFC et du CCl_4 dans l'étude de la circulation profonde de l'Atlantique Nord, Ph.D. thesis, Université de Bretagne Occidentale, Brest.

Fratantoni, D. M. (2001), North Atlantic surface circulation during the 1990s observed with satellite-tracked drifters, *J. Geophys. Res.*, *106*(C10), 22,067–22,094, doi:10.1029/2000JC000730.

Ganachaud, A. (2003), Error budget of inverse box models: The North Atlantic, *J. Atmos. Ocean. Technol.*, *20*(11), 1641–1655.

Ganachaud, A., and C. Wunsch (2003), Large-scale ocean heat and freshwater transports during the World Ocean Circulation Experiment, *J. Clim.*, *16*(2), 696–705.

Häkkinen, S., and P. B. Rhines (2004), Decline of subpolar North Atlantic, *Science*, *304*, 555–559.

Hansen, B., and S. Østerhus (2006), Monitoring the Faroe Bank Channel overflow, *Geophys. Res. Abstr.*, *8*, 06841.

Harvey, J. G., and A. Theodorou (1986), The circulation of Norwegian Sea overflow water in the eastern North Atlantic, *Oceanol. Acta*, *9*(4), 393–402.

Hátún, H., A. B. Sandø, H. Drange, B. Hansen, and H. Valdimarsson (2005), Influence of the Atlantic subpolar gyre on the thermohaline circulation, *Science*, *309*, 1841–1844, doi:10.1126/science.1114777.

Koltermann, K. P., A. V. Sokov, V. P. Tereschenkov, S. A. Dobroliubov, K. Lorbacher, and A. Sy (1999), Decadal changes in the thermohaline circulation of the North Atlantic circulation during the 1990s, *Science*, *46*, 109–138.

Krauss, W. (1995), Currents and mixing in the Irminger Sea and in the Iceland Basin, *J. Geophys. Res.*, *100*(C6), 10,851–10,871.

Lavender, K. L., R. E. Davis, and W. B. Owens (2000), Mid-depth recirculation observed in the interior Labrador and Irminger seas by direct velocity measurements, *Nature*, *407*, 66–69.

Lherminier, P., J.-P. Gouillou, C. Kermabon, and H. Mercier (2003), OVIDE 2002: Traitement des données des LADCP RDI-BB150 et RDI-WH300, *Tech. Rep. DRO/DOPS/LPO/03-10*, Ifremer.

Lux, M., H. Mercier, and M. Arhan (2000), Interhemispheric exchanges of mass and heat in the Atlantic Ocean in January–March 1993, *Deep Sea Res.*, *48*, 605–638.

Macrander, A., U. Send, H. Valdimarsson, S. Jonsson, and R. H. Käse (2005), Interannual changes in the overflows from the Nordic Seas into the Atlantic Ocean through Denmark Strait, *Geophys. Res. Lett.*, *32*, L06606, doi:10.1029/2004GL021463.

Marsh, R., B. A. de Cuevas, A. C. Coward, H. L. Bryden, and M. Alvarez (2005), Thermohaline circulation at three key sections in the North Atlantic over 1985–2002, *Geophys. Res. Lett.*, *32*, L10604, doi:10.1029/2004GL022281.

Maslowski, W., D. Marble, W. Walczowski, U. Schauer, J. L. Clement, and A. J. Semtner (2004), On climatological mass, heat and salt transports through the Barents Sea and Fram Strait from a pan-Arctic coupled ice-ocean model simulation, *J. Geophys. Res.*, *109*(C3), C03032, doi:10.1029/2001JC001039.

McCartney, M. S. (1992), Recirculating components to the deep boundary current of the northern North Atlantic, *Prog. Oceanogr.*, *29*(4), 283–383.

Mercier, H. (1986), Determining the general circulation of the ocean: A nonlinear inverse problem, *J. Geophys. Res.*, *91*(C4), 5103–5109.

Paillet, J., and H. Mercier (1997), An inverse model of the eastern North Atlantic general circulation and thermocline ventilation, *Deep Sea Res.*, *44*(8), 1293–1328.

Paillet, J., M. Arhan, and M. S. McCartney (1998), Spreading of Labrador Sea Water in the eastern North Atlantic, *J. Geophys. Res.*, *103*(C5), 10,223–10,239.

Pickart, R. S., F. Straneo, and G. W. K. Moore (2003), Is Labrador Sea Water formed in the Irminger Basin?, *Deep Sea Res.*, *50*(1), 23–52.

Pickart, R. S., D. J. Torres, and P. S. Fratantoni (2005), The East Greenland Spill Jet, *J. Phys. Oceanogr.*, *35*(6), 1037–1053, doi:10.1175/JPO2734.1.

Reverdin, G., P. P. Niiler, and H. Valdimarsson (2003), North Atlantic Ocean surface currents, *J. Geophys. Res.*, *108*(C1), 3002, doi:10.1029/2001JC001020.

Saunders, P. M. (1987), Flow through Discovery Gap, *J. Phys. Oceanogr.*, 631–643.

Saunders, P. M. (1994), The flux of overflow water through the Charlie Gibbs Fracture Zone, *J. Geophys. Res.*, *99*, 12,343–12,355.

Schmitz, W. J., Jr., and M. S. McCartney (1993), On the North Atlantic circulation, *Rev. Geophys.*, *31*(1), 29–49.

Schott, F., L. Stramma, and J. Fischer (1999), Interaction of the North Atlantic Current with the deep Charlie Gibbs Fracture Zone throughflow, *Geophys. Res. Lett.*, *26*, 369–372.

Serreze, M. C., A. P. Barrett, A. G. Slater, R. A. Woodgate, K. Aagaard, R. B. Lammers, M. Steele, R. Moritz, M. Meredith, and C. M. Lee (2006), The large-scale freshwater cycle of the Arctic, *J. Geophys. Res.*, *111*, C11010, doi:10.1029/2005JC003424.

Sy, A. (1988), Investigation of large-scale circulation patterns in the central North Atlantic Current, the Azores Current, and the Mediterranean Water plume in the area of the Mid–Atlantic Ridge, *Deep Sea Res.*, *35*, 383–413.

Treguier, A.-M., S. Theetten, E. Chassignet, T. Penduff, R. Smith, L. Talley, J. O. Beismann, and C. Böning (2005), The North Atlantic subpolar gyre in four high-resolution models, *J. Phys. Oceanogr.*, *35*(5), 757–774, doi:10.1175/JPO2720.1.

Treguier, A.-M., C. Gourcuff, P. Lherminier, H. Mercier, B. Barnier, G. Madec, J. Molines, T. Penduff, L. Czeschel, and C. Böning (2006), Internal and forced variability along a section between Greenland and Portugal in the CLIPPER Atlantic model, *Ocean Dyn.*, *56*(5-6), 568–580, doi:10.1007/s10236-006-0069-y.

Uppala, S., et al. (2005), The ERA-40 re-analysis, *Q. J. R. Meteorol. Soc.*, *131*, 2961–3012.

van Aken, H. M., and G. Becker (1996), Hydrography and through-flow in the north-eastern North Atlantic Ocean: The NANSEN project, *Prog. Oceanogr.*, *38*(4), 297–346, doi:10.1016/S0079-6611(97)00005-0.

Visbeck, M. (2002), Deep velocity profiling using Lowered Acoustic Doppler Current Profilers: Bottom track and inverse solutions, *J. Atmos. Ocean. Technol.*, *19*(5), 794–807.

Wilkinson, D., and S. Bacon (2005), The spatial and temporal variability of the East Greenland Coastal Current from historic data, *Geophys. Res. Lett.*, *32*, L24618, doi:10.1029/2005GL024232.

Woodgate, R. A., and K. Aagaard (2005), Revising the Bering Strait freshwater flux into the Arctic Ocean, *Geophys. Res. Lett.*, *32*, L02602, doi:10.1029/2004GL021747.

Wunsch, C., and P. Heimbach (2006), Estimated decadal changes in the North Atlantic Meridional Overturning Circulation and heat flux 1993–2004, *J. Phys. Oceanogr.*, *36*(11), 2012–2024, doi:10.1175/JPO2957.1.

M. Alvarez, IMEDEA (CSIC/UIB), Esporles, Mallorca, Spain.

S. Bacon, National Oceanographic Centre (NOC), Southampton, UK.

C. Gourcuff, C. Kermabon, P. Lherminier, and H. Mercier, Laboratoire de Physique des Océans, Ifremer, B.P. 70, 29280 Plouzané, France. (pascale.lherminier@ ifremer.fr)